Fully-Decoupled Radio Access Networks: A Resilient Uplink Base Stations Cooperative Reception Framework

Jiwei Zhao, *Member, IEEE*, Quan Yu, *Fellow, IEEE*, Bo Qian, *Member, IEEE*, Kai Yu, *Student Member, IEEE*, Yunting Xu, *Student Member, IEEE*, Haibo Zhou, *Senior Member, IEEE*, and Xuemin Shen, *Fellow, IEEE*

***Abstract*— To cope with the even more urgent spectrum and energy efficiency challenge for trillion-level terminal access and data uploading in the next generation mobile communication network (6G), in this paper, we investigate the uplink transmission in an original fully-decoupled radio access networks (FD-RAN) architecture. Specifically, we propose a resilient uplink base station cooperative reception framework in FD-RAN, which is a large-scale fading based two-tier signal combination approach for the uplink transmission, including the localized signal combination at the base station and centralized signal combination at the edge cloud, respectively. Then, we formulate a weighted sum-rate maximization problem for the uplink transmission optimization, and decompose it into two subproblems. A spectrum-efficiency maximized virtual service cluster selection (SEMVS) algorithm is designed by leveraging the channel statistical information for solving subproblem one, and a fractional programming based power control (FPPC) algorithm is introduced for the power optimization of subproblem two. Compared to the typical RAN architectures with corresponding access and power control methods, simulation results demonstrate the significant performance improvements of uplink FD-RAN with the proposed solution.**

***Index Terms*— FD-RAN, virtual service cluster, power control, spectrum efficiency, energy efficiency.**

Manuscript received 5 June 2022; revised 5 October 2022; accepted 11 December 2022. Date of publication 23 January 2023; date of current version 14 August 2023. This work was supported in part by the National Natural Science Foundation Original Exploration Project of China under Grant 62250004, in part by the National Natural Science Foundation of China under Grant 62271244, in part by the Natural Science Fund for Distinguished Young Scholars of Jiangsu Province under Grant BK20220067, and in part by the Natural Sciences and Engineering Research Council of Canada (NSERC). The associate editor coordinating the review of this article and approving it for publication was S. Zhou. *(Corresponding author: Haibo Zhou.)*

Jiwei Zhao, Kai Yu, and Yunting Xu are with the School of Electronic Science and Engineering, Nanjing University, Nanjing 210023, China (e-mail: jw_zhao@smail.nju.edu.cn; kaiyu@smail.nju.edu.cn; yuntingxu@smail.nju.edu.cn).

Quan Yu and Haibo Zhou are with the School of Electronic Science and Engineering, Nanjing University, Nanjing 210023, China, and also with the Peng Cheng Laboratory, Shenzhen 518000, China (e-mail: yuquan61@qq.com; haibozhou@nju.edu.cn).

Bo Qian is with the Department of Mathematics and Theories, Peng Cheng Laboratory, Shenzhen 518000, China (e-mail: boqian@pcl.ac.cn).

Xuemin Shen is with the Department of Electrical and Computer Engineering, University of Waterloo, Waterloo, ON N2L 3G1, Canada (e-mail: sshen@uwaterloo.ca).

Color versions of one or more figures in this article are available at https://doi.org/10.1109/TWC.2022.3231625.

Digital Object Identifier 10.1109/TWC.2022.3231625

I. Introduction

As a vital enabler for the future intelligent information society, the six-generation mobile communication networks (6G) are expected to provide higher spectrum efficiency (SE), higher energy efficiency (EE), and a more personalized user experience [1], [2], [3], [4]. It will connect everything, provide full-dimensional green/economical coverage, and integrate various functions, including sensing, computing, caching, communication, etc. However, confronted with trillion-level massive access and asymmetry quality of service requirements for uplink and downlink in the incoming digitized society, how to achieve efficient network resources utilization and realize cost-effective network operation, will be of great challenge [5], [6], [7], [8]. To meet these challenges, an original network architecture, namely, the fully-decoupled radio access networks (FD-RAN) [2], was proposed and has attracted considerable attention from industry and academia.

The FD-RAN is essentially a cloud radio access network (C-RAN) architecture with the complete physical decoupling of network resources. In the FD-RAN, base stations (BSs) are decoupled into control BSs and data BSs, and data BSs are further decoupled into independently deployed uplink base stations (UBSs) and downlink base stations (DBSs). By virtue of the physically decoupling of UBS and DBS, the uplink transmission and downlink transmission can be separated, which can further break through the constraint that users should access the same BS both in uplink and downlink transmission. Besides, the decoupling of data BSs allows us to flexibly deploy UBSs and DBSs according to the user service requirements in the coverage area. After that, the collaboration of multiple BSs to provide personalized services for each user has become the default operation mode in stand-alone uplink networks or downlink networks. Moreover, the control BS acts as the controller of uplink networks and downlink networks for resource cooperation. Consequently, the new transmission model with limited and delayed feedback and the scheduling of decoupled uplink and downlink resources become vital challenges in FD-RAN networks, which decides the upper bound performance. Especially, in light of the explosive growth of uplink traffic and the proliferation of

1536-1276 © 2023 IEEE. Personal use is permitted, but republication/redistribution requires IEEE permission.
See https://www.ieee.org/publications/rights/index.html for more information.

Authorized licensed use limited to: University of Waterloo. Downloaded on August 20,2023 at 10:02:36 UTC from IEEE Xplore. Restrictions apply.

massive low-power access points, it is crucial to investigate the cooperation among multiple UBSs in uplink networks in order to meet the growing need for uplink services.

Cooperative communication has been proven to be an effective technology to improve user service when dealing with the scarcity of the radio spectrum [9], [10]. In the uplink FD-RAN, each user will be served with cooperative joint reception by multiple UBSs. Although single BS reception has been well investigated, how to schedule partial UBSs to serve every user in FD-RAN remains a major challenge, especially considering fronthaul and fairness limitations.

The large-scale fading decoding (LSFD) [11] technique, which combines signals from multiple BSs to reduce inter-user interference, is suitable for scenarios with massive access and ultra-reliable service requirements. It can obtain the beamforming gain from the combination of multiple antenna signals and the diversity gain from the combination of multiple BS signals, which not only promotes the network throughout but also guarantee user access service. In addition, the power control can reduce the interference between users with a centralized optimization algorithm, and then improve network SE. It can also reduce the overall power consumption compared to the maximum power transmitting scheme, which deserves further research for achieving a better balance between SE and EE. In this paper, we model the joint reception with the LSFD technique, and propose the non-convex uplink weighted sum-rate (WSR) maximization optimization problem. In order to find a low-complexity and practically feasible solution, the original optimization problem is decomposed into two subproblems, namely, the virtual access and the uplink power control. Then, we firstly develop a novel solution on the basis of marginal effects for the virtual access problem, and propose an iterative algorithm based on proportional programming for the uplink power control. The major contributions are summarized as follows.

- We propose a large-scale fading decoding based two-tier signal combination approach in uplink FD-RAN, in which every UBS will firstly process the received signal from multiple antennas, and then send the processed signal to the edge cloud for further decoding. The two-tier signal combination scheme is capable of reducing information redundancy and improving transmission efficiency.
- We formulate a general WSR maximization problem to jointly optimize the user virtual service cluster (VSC) selection among the cooperative UBSs and user power control. An effective SE maximized VSC selection (SEMVS) algorithm is designed to reduce the network fronhaul load with limited SE sacrifice.
- We design a fractional programming based power control (FPPC) algorithm to iteratively solve the non-convex WSR maximization problem so as to reduce the overall user uplink transmission power. With the optimized power control, the energy efficiency will be significantly improved and finally facilitate the enhancement of spectrum efficiency.

The remainder of the paper is organized as follows. In Section II, we summarize the related work on uplink association and power control. We describe the system model and propose the problem of joint optimization of VSC selection and uplink power control in Section III. Then, the SEMVS and FPPC algorithms are proposed in Section IV. Besides, the simulation setup and numerical results are presented in Section V. Finally, we conclude this paper in Section VI.

II. Related Works

Recently, with the introduction of C-RAN [12], distributed antenna system (DAS) [13], and cell-free network [14], how to excavate the full potential of BSs cooperation from the perspective of network architecture has been extensively studied. In the DAS, the BS with a single high-power antenna is replaced by a group of low-power antenna elements separated in the same area, so as to provide improved coverage but with reduced transmit power and enhanced reliability. In the C-RAN, a series of remote radio heads (RRHs), which perform radio functionalities (i.e., frequency up/down conversion, and A/D and D/A conversion), are geographically distributed in the coverage area. In the cell-free network, a group of distributed access points (APs) cooperates to serve all active users within the network coverage area simultaneously using the same frequency-time resources [15].

In particular, for the uplink cooperation reception, minimum mean-square error (MMSE), which is a linear optimal local decoding method and can simultaneously reduce inter-user interference [16], is ideally suited for scenarios requiring massive access and highly reliable service when compared to maximum ratio combining (MRC) and zero-forcing (ZF). Moreover, the benefits of centralized MMSE combination were proven for the enhancement of SE and EE [14], [15], [17]. Although the centralized MMSE combination has an attractive performance, it is hard to be accomplished for the original cell-free scenario, where all APs jointly receive signals from all users [14], due to the constraints of computation, fronthaul load and etc. [18], [19], [20]. Then, the partial MMSE was proposed for cutting down the computation complexity [15]. However, the centralized MMSE combination needs to compute the inversion of the channel matrix with the $O\left(n^3\right)$ complexity, which is unscalable with the increase of service UBSs or antennas. Demir et al. analyzed the performance of several fully-distributed methods, i.e., ZF and MRC [16]. As a compromise, the LSFD technique had been proposed and attracted plenty of attention for the balance of performance and complexity [11]. In the LSFD, signals from multiple BSs are joint-decoded according to large-scale fading for higher performance than a single BS.

For intensively deployed uplink FD-RAN, the contribution of different UBSs to the SE is different due to the time-varying fading channel. According to the research in [21], we can deduce that just 10-20% of the UBSs could receive more than 95% of the total power for each user in a $1\ \mathrm{km}^2$ square area. In order to overcome the complexity caused by all BSs serving all users, there are intensive works concentrating on selecting partial UBSs to serve users. Björnson et al. proposed a scalable access and pilot allocation integrating scenario [15]. Zaidi et al. introduced a virtualization access approach, which

Authorized licensed use limited to: University of Waterloo. Downloaded on August 20,2023 at 10:02:36 UTC from IEEE Xplore. Restrictions apply.

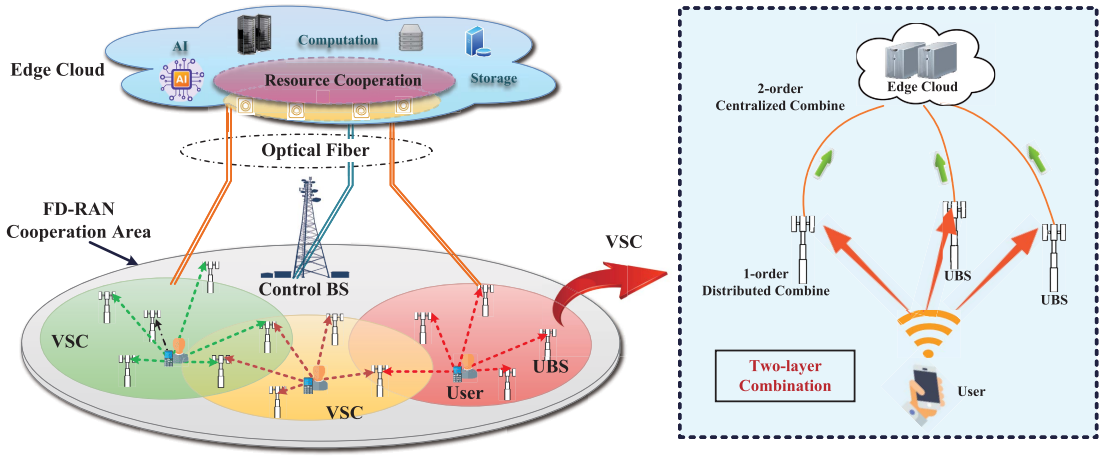

Fig. 1. Proposed resilient UBSs cooperative reception framework.

selects partial service APs according to large-scale channels, to promote the network performance [22]. Besides, there are many constraints that influence the UBSs subset selection, such as fronthaul load, quality of service, and bandwidth occupation [23].

Additionally, different power optimization techniques based on maximizing the WSR or Max-Min signal to interference and noise ratio (SINR) were proposed [24], [25], [26], [27], [28], [29], [30], [31]. Max-Min SINR optimization has the advantage of providing as good service as possible for users who undergo the worst channel, which attracted lots of research interests [24], [25]. Globally optimal schemes to solve WSR optimization problems have also been studied recently [26], [27], [28]. Shi et al. developed the WMMSE algorithm [30], in which the equivalence of minimizing the weighted minimum mean square error (MSE) and maximizing the WSR is proved, and a block coordinate descent strategy is proposed for the original WSR problem. Shen et al. proposed another excellent fractional programming based weighted sum-rate approach, which demonstrates a faster iteration convergency [29], [31]. Moreover, the joint optimization of UBS selection and power control has also been initially studied [23], [32], [33], [34]. The authors in [23] proposed an iterative power control and access point scheduling framework. Dong et al. employed the iterative successive convex approximation to maximize the system EE with respect to the power control, the antenna activation, and the RRH-user association in a combinatorial manner [32]. Moreover, [33], [34] validated that the combination of power control and association can promote SE, EE, and load balancing.

III. System Model and Problem Formulation

A. Overview of the Uplink FD-RAN Network

Fig. 1 illustrates the resilient UBSs cooperative reception framework. The uplink network contains the physically separated control BS and UBSs, in which all users are served by cooperated multiple UBSs. The control BS is the controller and coordinator for all UBSs and users located in the FD-RAN. All UBSs and the control BS are connected to the edge cloud via low-latency fiber optics. We propose a two-tier signal combination framework for FD-RAN uplink transmission, which is comprised of the localized signal combination at each UBS, and the centralized signal combination at the edge cloud. As illustrated in Fig. 1, users usually transmit data signals to a cluster of UBSs, where the received signals from multiple antennas will firstly be implemented in the first-tier combination, and then be forwarded to the edge cloud for the second-tier processing. In addition, the channel statistical information collected in UBS will be periodically transmitted to the edge cloud. Consequently, the edge cloud will always hold global channel information, which is conducive to the combining of signals for UBSs in the cooperative VSC.

B. Channel Model and Channel Estimation

We concentrate on the uplink transmission scenario in the FD-RAN, where there are M randomly distributed N-antenna UBSs serving K randomly distributed single-antenna users. We assume the channel response $\mathbf{h}_{m,k}$ between user k and the UBS m follows the spatially correlated Rayleigh distribution $\mathbf{h}_{m,k} \sim \mathcal{N}_{\mathbb{C}}\left(0, \mathbf{R}_{m,k}\right)$, namely, the channel is sampled from the circularly symmetric complex Gaussian distribution. Each element of $\mathbf{h}_{m,k}$ corresponds to an antenna in UBS m. Additionally, we assume that the channels between user k to any different two UBSs are independently distributed. Based on the spatial independence of different UBSs, it holds that $\mathbb{E}\left\{\left(\mathbf{h}_{m,k}\right)\left(\mathbf{h}_{l,k}\right)^{\mathrm{H}}\right\} = \mathbf{0}$ for $m \neq l$. Then, the collective channel of user k satisfies

$$\mathbf{h}_k \sim \mathcal{N}_{\mathbb{C}}\left(\mathbf{0}, \mathbf{R}_k\right), \tag{1}$$

where $\mathbf{R}_k = \operatorname{diag}\left(\mathbf{R}_{1,k}, \ldots, \mathbf{R}_{m,k}\right) \in \mathbb{C}^{MN \times MN}$ is a block-diagonal matrix denoting the spatial correlations of different channels. Besides, we suppose that the spatial correlation matrices $\boldsymbol{R}_{m,k}$ can always be acquired both in UBS and edge cloud. And, the average gain $\beta_{m,k}$ for the channel between the user k to the UBS m is determined by the normalized trace

$$\beta_{m,k} = \operatorname{tr}\left(\mathbf{R}_{m,k}\right)/N, \tag{2}$$

Authorized licensed use limited to: University of Waterloo. Downloaded on August 20,2023 at 10:02:36 UTC from IEEE Xplore. Restrictions apply.

which reflects the large-scale fading of the channel $\mathbf{h}_{m,k}$. We assume that the channel $\mathbf{h}_{m,k}$ remains constant over a coherence block τ_c, which is divided to two parts $\tau_c = \tau_p + \tau_u$, with one for pilots (τ_p) and the remainder for uplink data transmission (τ_u). All realizations of channels between any pair of coherence blocks are independent. We assume there are τ_p mutually orthogonal pilot signals $\boldsymbol{\varphi}_1, \ldots, \boldsymbol{\varphi}_{\tau_p} \in \mathbb{C}^{\tau_p \times 1}$, where τ_p is a constant independent of K. Any pilot is qualified with $|\boldsymbol{\varphi}_t|^2 = \tau_p$ for $t = 1, \ldots, \tau_p$. Furthermore, the pilots satisfy

$$\boldsymbol{\varphi}_{t_1}^{\mathrm{H}} \boldsymbol{\varphi}_{t_2} = \begin{cases} \tau_p & \text{if } t_1 = t_2 \\ 0 & \text{if } t_1 \neq t_2. \end{cases} \tag{3}$$

The pilots are allocated to users in a dynamic cluster manner [15]. The user set, where all users employ the same pilot t_k, is expressed as $\mathcal{P}_k = \left\{ i : \boldsymbol{\varphi}_{t_k} = \boldsymbol{\varphi}_{t_i}, 1 \leq i \leq K \right\}$. We assume that user k transmits pilot $\sqrt{\rho_k}\boldsymbol{\varphi}_{t_k}$, where ρ_k denotes the pilot transmission power of k. Then, the UBS m will receive the pilot signal

$$\mathbf{y}_m^p = \sum_{k=1}^{K} \sqrt{\rho_k}\, \mathbf{h}_{m,k} \boldsymbol{\varphi}_{t_k}^{\mathrm{H}} + \mathbf{n}_m, \tag{4}$$

where $\mathbf{n}_m \sim \mathcal{N}_{\mathbb{C}}\left(\mathbf{0}, \sigma^2 \mathbf{I}_N\right)$ is the Gaussian white noise. In order to estimate the channel $\mathbf{h}_{m,k}$, we define the pilot signal received at UBS m for user k as

$$\begin{aligned} \mathbf{y}_{m,k}^p &\triangleq \frac{1}{\sqrt{\tau_p}} \mathbf{y}_m^p \boldsymbol{\varphi}_{t_k}^{\mathrm{H}} = \sum_{i=1}^{K} \frac{\sqrt{\rho_i}}{\sqrt{\tau_p}} \mathbf{h}_{m,i} \boldsymbol{\varphi}_{t_i}^{\mathrm{H}} \boldsymbol{\varphi}_{t_k}^{\mathrm{H}} + \frac{1}{\sqrt{\tau_p}} \mathbf{n}_m \boldsymbol{\varphi}_{t_k}^{\mathrm{H}} \\ &= \sum_{i \in \mathcal{P}_k} \sqrt{\rho_i \tau_p} \mathbf{h}_{m,i} + \hat{\mathbf{n}}_{m,k}. \end{aligned} \tag{5}$$

Leveraging the typical MMSE method [15], the estimation of $\mathbf{h}_k$ can be denoted as

$$\hat{\mathbf{h}}_{m,k} = \frac{\sqrt{\tau_p \rho_k} \mathbf{R}_{m,k} \mathbf{y}_{m,k}^p}{\sum_{i \in \mathcal{P}_k} \tau_p \rho_i \mathbf{R}_{m,i} + \delta^2 \mathbf{I}_N}, \tag{6}$$

Thus, we can obtain the correlation matrix of estimation error

$$\begin{aligned} \mathbf{C}_{m,k} &= \mathbb{E}\left\{ \left(\mathbf{h}_{m,k} - \hat{\mathbf{h}}_{m,k} \right) \left(\mathbf{h}_{m,k} - \hat{\mathbf{h}}_{m,k} \right)^{\mathrm{H}} \right\} \\ &= \mathbf{R}_{m,k} - \tau_p \rho_k \mathbf{R}_{m,k} \left(\sum_{i \in \mathcal{P}_k} \tau_p \rho_i \mathbf{R}_{m,i} + \sigma^2 \mathbf{I}_N \right)^{-1} \mathbf{R}_{m,k}. \end{aligned} \tag{7}$$

C. Two-Tier Combination Based Uplink Data Transmission

For the uplink transmission, we assume that user k transmits symbol q_k, which satisfies $\mathbb{E}\{q_k\} = 0$, and $\mathbb{E}\left\{|q_k|^2\right\} = 1$. Thus, UBS m will received the mixed signal from all users

$$\mathbf{y}_m = \sum_{k=1}^{K} \sqrt{\eta_k} \mathbf{h}_{m,k} q_k + \mathbf{n}_m, \tag{8}$$

where $\eta_k \leq 0$ denotes the data transmission power. Considering the fronthaul overhead, we assume each BS will schedule a subset of users $\mathcal{K}_m$. Then, we define the variable $x_{m,k}$ to denote whether UBS m serves user k

$$x_{m,k} = \begin{cases} 1 & m \to k \\ 0 & \text{others}, \end{cases} \tag{9}$$

where $x_{m,k}$ is 1 if m is expected to decode signal for user k ($m \to k$) and 0 otherwise. Specifically, we assume that every UBS can serve no more than $\mathcal{K}_T$ users [23], [35], where the $\mathcal{K}_T$ is a hyperparameter specified by the fronthaul bandwidth. In addition, considering the fairness between different users, we assume that every user will employ at most $\mathcal{M}_T$ UBSs. Naturally, the subset of UBS that serve user k can be defined as $\mathcal{M}_k = \{m : x_{m,k} = 1, k \in \{1, \ldots, K\}\}$. In addition, the user subset that is served by UBS m can be expressed as $\mathcal{K}_m = \{k : x_{m,k} = 1, k \in \{1, \ldots, K\}\}$.

Here, we put forward a two-tier signal combination framework based on LSFD for uplink joint reception. We assume every UBS will firstly receive signals with multiple antennas and implement local combination. Then, the combined signal will be transmitted to the edge cloud. Thereafter, signals from multiple UBSs would be jointly decoded according to corresponding channel statistics information.

1) Localized Combination: As for user k, the service UBS m will implement a real-time local combination for multiple antennas with the decoding vector $\mathbf{w}_{m,k}$. Then, the local symbol estimation of q_k can be expressed as $\hat{q}_{m,k} = x_{m,k} \mathbf{w}_{m,k}^{\mathrm{H}} \mathbf{y}_{m,k}$, where $x_{m,k}$ is a long-term variable corresponding to large-scale channel, and determined by the edge cloud controller. By minimizing the MSE between q_k and $\mathbf{w}_{m,k}^{\mathrm{H}} \mathbf{y}_{m,k}$ given channel estimation $\hat{h}_{m,k}$, we can acquire the MMSE combination vector

$$\begin{aligned} \mathbf{w}_{m,k} &= \underset{\mathbf{w}_{m,k}}{\arg\min} \mathbb{E}\left\{ \left| q_k - \mathbf{w}_{m,k}^{\mathrm{H}} \mathbf{y}_m \right|^2 \mid \left\{ \hat{\mathbf{h}}_{m,k} \right\} \right\} \\ &= \rho_k \left(\sum_{i=1}^{K} \rho_i \left(\hat{\mathbf{h}}_{m,i} \hat{\mathbf{h}}_{m,i}^{\mathrm{H}} + \mathbf{C}_{m,i} \right) + \sigma^2 \mathbf{I}_N \right)^{-1} \hat{\mathbf{h}}_{m,k}. \end{aligned} \tag{10}$$

2) Centralized Combination: Then, we will combine all received signals from UBSs belonging to $\mathcal{M}_k$ for any served user k with the centralized combination vector $\alpha_{m,k}$

$$\begin{aligned} \hat{q}_k = \sqrt{\eta_k} &\left(\sum_{m \in \mathcal{M}_k} \alpha_{m,k}^* \mathbf{w}_{m,k}^{\mathrm{H}} \mathbf{h}_{m,k} \right) q_k \\ &+ \sum_{i=1, i \neq k}^{K} \sqrt{\eta_i} \left(\sum_{m \in \mathcal{M}_k} \alpha_{m,k}^* \mathbf{w}_{m,k}^{\mathrm{H}} \mathbf{h}_{m,i} \right) q_i + n_k'. \end{aligned} \tag{11}$$

Specifically, the last term $n_k' = \sum_{m=1}^{M} \alpha_{m,k} x_{m,k} \mathbf{w}_{m,k}^{\mathrm{H}} \mathbf{n}_m$ denotes the weighted noise sum. Then, we can rewrite (11) to the effective channel expression

$$\widehat{q_k} = \underbrace{\sqrt{\eta_k} \boldsymbol{\alpha}_k^{\mathrm{H}} \mathbf{g}_{kk} q_k}_{\text{Desired signal}} + \underbrace{\sum_{i=1, i \neq k}^{K} x_{m,k} \sqrt{\eta_i} \boldsymbol{\alpha}_k^{\mathrm{H}} \mathbf{g}_{ki} q_i}_{\text{Interference}} + \underbrace{n_k'}_{\text{Noise}}. \tag{12}$$

As shown in (12), the signal after the first-tier combination can be regarded as an effective signal received by $|\mathcal{M}_k|$ antennas in a single UBS. Then, we can define the effective

Authorized licensed use limited to: University of Waterloo. Downloaded on August 20,2023 at 10:02:36 UTC from IEEE Xplore. Restrictions apply.

channel from user k to all UBSs in $\mathcal{M}_k$ as

$$\mathbf{g}_{k,i} \triangleq \left[\mathbf{w}_{t_1,k}^{\mathrm{H}}\mathbf{h}_{t_1,i},\ldots,\mathbf{w}_{t_{|\mathcal{M}_k|},k}^{\mathrm{H}}\mathbf{h}_{t_{|\mathcal{M}_k|},i}\right]^{\mathrm{T}}, \tag{13}$$

where $|\mathcal{M}_k|$ is the number of elements of set $\mathcal{M}_k$, and t_m indicates the index of the m-th UBS in $\mathcal{M}_k$. The m-th element in $\mathbf{g}_{k,i}$ is $\mathbf{g}_{k,i}^{(m)} = \mathbf{w}_{t_m,k}^{\mathrm{H}}\mathbf{h}_{t_m,i}$. Then, we further define the combination vector $\boldsymbol{\alpha}_k \in \mathbb{C}^{|\mathcal{M}_k|\times 1}$ for user k

$$\boldsymbol{\alpha}_k \triangleq \left[\alpha_{t_1,k},\ldots,\alpha_{t_{|\mathcal{M}_k|},k}\right]^{\mathrm{T}}. \tag{14}$$

From another perspective, both $\mathbf{g}_{k,i}$ and α_k are functions of $\mathbf{X}$, which should be denoted by $\mathbf{g}_{k,i}(\mathbf{X})$ and $\alpha_k(\mathbf{X})$. However, we still use the original formation of $\mathbf{g}_{k,i}$ and α_k for a compact expression. Although the real-time and deterministic channel $\boldsymbol{\alpha}_k^{\mathrm{H}}\mathbf{g}_{k,i}$ cannot be known in the cloud, its expectation $\boldsymbol{\alpha}_k^{\mathrm{H}}\mathbb{E}\{\mathbf{g}_{ki}\}$ is able to be acquired with periodically uplink transmission [15]. According to the inference of use-and-then-forget (UatF) bound [16], the achievable SINR for user k can be written as

$$\phi_k = \frac{\eta_k\left|\boldsymbol{\alpha}_k^{\mathrm{H}}\mathbb{E}\{\mathbf{g}_{kk}\}\right|^2}{\boldsymbol{\alpha}_k^{\mathrm{H}}\left(\sum_{i=1}^{K}\eta_i\mathbb{E}\{\mathbf{g}_{ki}\mathbf{g}_{ki}^{\mathrm{H}}\}-\eta_k\mathbb{E}\{\mathbf{g}_{kk}\}\mathbb{E}\{\mathbf{g}_{kk}^{\mathrm{H}}\}+\mathbf{N}_k\right)\boldsymbol{\alpha}_k}, \tag{15}$$

where $\mathbf{N}_k = \mathrm{diag}\left(\sigma^2\mathbb{E}\left\{\left\|\mathbf{w}_{t_1,k}^{\mathrm{H}}\right\|^2\right\},\ldots,\sigma^2\mathbb{E}\left\{\|\mathbf{w}_{t_{|\mathcal{M}_k|},k}^{\mathrm{H}}\|^2\right\}\right)$ means the effective noise power diagonal matrix. In addition, expectation terms $\mathbb{E}\{\mathbf{g}_{kk}\}$ and $\mathbb{E}\{\mathbf{g}_{ki}\mathbf{g}_{ki}^{\mathrm{H}}\}$ can be obtained through periodic statistics of UBSs.

D. Problem Formulation

In this paper, we target to determine the service UBS subset and transmission power for users to maximize the WSR. Then, a network utility function, namely, the weighted-sum-rates maximization, is proposed for the FD-RAN uplink transmission. According to [16], the effective MMSE-based optimal centralized combination vector $\boldsymbol{\alpha}$ can be acquired:

$$\begin{aligned}\boldsymbol{\alpha}^{\star} &= \arg\max_{\boldsymbol{\alpha}}\ \phi_k \\ &= \left(\sum_{i=1}^{K}\eta_i\mathbb{E}\left\{\mathbf{g}_{ki}\mathbf{g}_{ki}^{\mathrm{H}}\right\}-\eta_k\mathbb{E}\{\mathbf{g}_{kk}\}\mathbb{E}\left\{\mathbf{g}_{kk}^{\mathrm{H}}\right\}+\mathbf{N}_k\right)^{-1} \\ &\quad\times\mathbb{E}\{\mathbf{g}_{kk}\}.\end{aligned} \tag{16}$$

For notation clarity, we utilize $\Phi_k\{\hat{\mathbf{X}},\boldsymbol{\eta},\boldsymbol{\alpha}^{\star}\}$ to represent the SINR for user k. Substituting $\boldsymbol{\alpha}$ with the proposed centralized combination vectors $\boldsymbol{\alpha}^{\star}$, the optimal SINR for user k depicted in (15) can be rewritten as

$$\begin{aligned}\Phi_k\{\mathbf{X},\boldsymbol{\eta},\boldsymbol{\alpha}^{\star}\} = \eta_k\mathbb{E}\left\{\mathbf{g}_{kk}^{\mathrm{H}}\right\}\Bigg(\sum_{i=1}^{K}\eta_i\mathbb{E}\left\{\mathbf{g}_{ki}\mathbf{g}_{ki}^{\mathrm{H}}\right\}-\eta_k\mathbb{E}\{\mathbf{g}_{kk}\} \\ \times\mathbb{E}\left\{\mathbf{g}_{kk}^{\mathrm{H}}\right\}+\mathbf{N}_k\Bigg)^{-1}\mathbb{E}\{\mathbf{g}_{kk}\},\end{aligned} \tag{17}$$

which is only correlated to the association decisions $\mathbf{X}$ and transmission powers $\boldsymbol{\eta}$ for all users. Given a set of weights $v_1,\ldots,v_K$ that reflect the users' priorities for scheduling, the optimization problem of WSR maximization can be modeled as

$$\max_{\mathbf{X},\boldsymbol{\eta}}\ \sum_{k=1}^{K}v_k\log_2\left(1+\Phi\{\mathbf{X},\boldsymbol{\eta},\boldsymbol{\alpha}^{\star}\}\right) \tag{18a}$$

$$\text{s.t. } 0\le\eta_k\le\eta_{\max}, \tag{18b}$$

$$\sum_{k=1}^{K}x_{m,k}\le\mathcal{K}_T, \tag{18c}$$

$$\sum_{m=1}^{M}x_{m,k}\le\mathcal{M}_T, \tag{18d}$$

$$x_{m,k}\in\{0,1\},\quad\forall m\in\mathcal{M},\quad\forall k\in\mathcal{K}, \tag{18e}$$

where (18b) means that the transmission power is larger than zero and is up to $\eta_{\max}$ for the reason of physical power constraints of users. (18c) and (18d) correspond to fronthaul and fairness limitations, respectively. The constraint in (18e) enforces the scheduling decisions to be binary. Namely, a user is scheduled if its scheduling variable equals one, and vice versa.

We find that the optimization problem (18a) has a mixed binary integer formation and is nonconvex with the power control variables. In fact, as mentioned above, the general WSR maximization problem has been shown to be NP-hard by Luo and Zhang in [30]. To solve this problem and obtain an effective solution, we divide the problem (18a) into two sub-problems, (19a) and (20a), to decouple the optimization of binary variables $\mathbf{X}$ and continuous variable $\boldsymbol{\eta}$. The sub-problem (19a), which concentrates on the UBS selection based on the effective spectrum efficiency maximization, can be formulated as

$$\max_{\mathbf{X}}\ \sum_{k=1}^{K}v_k\log_2\left(1+\Phi_k\{\mathbf{X},\hat{\boldsymbol{\eta}},\boldsymbol{\alpha}^{\star}\}\right) \tag{19a}$$

$$\text{s.t. } \sum_{k=1}^{K}x_{m,k}\le\mathcal{K}_T, \tag{19b}$$

$$\sum_{m=1}^{M}x_{m,k}\le\mathcal{M}_T, \tag{19c}$$

$$x_{m,k}\in\{0,1\},\quad\forall m\in\mathcal{M},\quad\forall k\in\mathcal{K}, \tag{19d}$$

in which, $\hat{\boldsymbol{\eta}}$ means the power control variables are fixed. Besides, the sub-problem (20a) focuses on solving the user's transmit power optimization with fixed virtual association decisions $\hat{\mathbf{X}}$

$$\max_{\boldsymbol{\Gamma},\boldsymbol{\eta}}\ \sum_{k=1}^{K}v_k\log_2\left(1+\Phi_k\{\hat{\mathbf{X}},\boldsymbol{\eta},\boldsymbol{\alpha}^{\star}\}\right) \tag{20a}$$

$$\text{s.t. } 0\le\eta_k\le\eta_{\max},\quad\forall\ k\in\mathcal{K}. \tag{20b}$$

IV. Virtual Service Cluster Selection and Uplink Power Control

In (17), the second-order statistics $\mathbb{E}\{\mathbf{g}_{ki}\mathbf{g}_{ki}^{\mathrm{H}}\}$ cannot be directly obtained by only one BS since $\mathbb{E}\{\mathbf{g}_{k,i}^{(m_1)}\mathbf{g}_{k,i}^{*(m_2)}\}$ for $m_1\neq m_2$ involves two different UBSs. However, considering

Authorized licensed use limited to: University of Waterloo. Downloaded on August 20,2023 at 10:02:36 UTC from IEEE Xplore. Restrictions apply.

that the spatial correlation matrix $\mathbf{R}_k$ is a block-diagonal matrix, in other words, the channels between any different UBSs are mutually independent, we can acquire the following expectation

$$\mathbb{E}\left\{\mathbf{g}_{k,i}^{(m_1)}\mathbf{g}_{k,i}^{*(m_2)}\right\} \approx \begin{cases} \mathbb{E}\left\{\mathbf{g}_{k,i}^{(m_1)}\right\}\mathbb{E}\left\{\mathbf{g}_{k,i}^{*(m_2)}\right\} & m_1 \neq m_2 \\ \mathbb{E}\left\{\|\mathbf{g}_{k,i}^{(m_1)}\|^2\right\} & m_1 = m_2. \end{cases} \tag{21}$$

where $\mathbf{g}_{k,i}^{(m)} = \mathbf{w}_{t_1,k}^{\mathrm{H}}\mathbf{h}_{t_1,i}$ denotes the m_{th} element of $\mathbf{g}_{ki}$. Therefore, $\mathbb{E}\left\{\mathbf{g}_{ki}\mathbf{g}_{ki}^{\mathrm{H}}\right\}$ can be rewritten to (22), shown at the bottom of the page, where $\mathrm{diag}\{\mathbf{A}\}$ is the diagonal matrix of matrix/vector $\mathbf{A}$ while $\mathbb{D}\{\mathbf{A}\}$ denotes its variance.

Applying (22) to (16), the MMSE-based centralized effective combination vector can be further rewritten as

$$\boldsymbol{\alpha}_k^{\star} = \left(\sum_{i=1}^{K}\eta_i\mathbb{E}\left\{\mathbf{g}_{ki}\right\}\mathbb{E}\left\{\mathbf{g}_{ki}^{\mathrm{H}}\right\} + \sum_{i=1}^{K}\eta_i\mathrm{diag}\left\{\mathbb{D}\left\{\mathbf{g}_{\mathrm{ki}}\right\}\right\} + \mathbf{N}_k\right)^{-1}\mathbb{E}\left\{\mathbf{g}_{kk}\right\}. \tag{23}$$

Based on the secondary combination vector (23), and applying (22) to (17), the effective SINR can be converted to (24), shown at the bottom of the page,.

In the following, we will firstly decide on the UBS association policy, $\hat{\mathbf{X}}$, and then optimize the transmission power for all users based on the solved association decisions.

A. Effective Spectrum Efficiency Maximized VSC Selection

The UBS selection problem mainly contains two stages. First of all, each UBS will individually estimate its first-order and second-order statistics, and then transmit uplink statistical information to the edge cloud. Afterward, the edge cloud will solve the UBS selection problem with the provided information.

1) Statistics of Effective Channel: First of all, each UBS estimates its channel based on the received pilot signal. In general, any UBS m will ignore those users whose channel to UBS m is terrible. Before determining the VSC, we will firstly define the channel fading threshold T_R, which means that the users whose channel fading to m lower than the T_R will not be served. Then, the users, whose large-scale channel fading to UBS m is higher than T_R, will come into being a candidate service set $\mathcal{K}_m^c$. Thereafter, the UBS can only compute $w_{m,k}$ for those users belonging to $\mathcal{K}_m^c$, which can significantly cut down the computation complexity and save energy during UBSs selection and network operation. Accordingly, only partial estimation of $\mathbf{g}_{k,i}$ will be utilized to obtain $\boldsymbol{\alpha}_k^{mmse}$ and $\Phi_k\{\mathbf{X}, \hat{\boldsymbol{\eta}}\}$. Hence, each UBS will only estimates the statistical information $\mathbb{E}\{\|\mathbf{w}_{m,k}^{\mathrm{H}}\|^2\}$, $\mathbb{E}\{\mathbf{g}_{ki}^{(m)}\}$, and $\mathbb{D}\left\{\mathbf{g}_{ki}^{(m)}\right\}$ for those users belonging to $\mathcal{M}_k^c$, and then upload it to the edge cloud. Moreover, if we get $\mathcal{K}_m^c$, the candidate uplink service UBSs subset $\mathcal{M}_k^c = \{m | k \in \mathcal{K}_m^c, m = 1, \ldots, M\}$ for user k can be acquired.

Different from the LSFD proposed in [15], the channel statistics transmitted to the cloud, enable the edge cloud to obtain the global statistical information, which will allow the network to make global scheduling decisions. Compared with [15], the proposed method can decrease computation cost of the edge cloud for the localized computation of variance $\mathbb{D}\{\mathbf{g}_{ki}\}$. Then, we described how to acquire the statistics of the effective channel in Algorithm 1, which is executed at each UBS m in $\mathcal{M}$.

Algorithm 1 Localized Statistics of Effective Channel

Input: $\mathbf{R}_{m,k}$, $m \in \{1, \ldots, M\}, k \in \{1, \ldots, K\}$
Output: $\mathbb{E}\{\|\mathbf{w}_{m,k}^{\mathrm{H}}\|^2\}$, $\mathbb{E}\{\mathbf{g}_{ki}^{(m)}\}$, and $\mathbb{D}\left\{\mathbf{g}_{ki}^{(m)}\right\}$

1: **parallel** for m in $\mathcal{M}$ **do:**
2: Determine $\mathcal{K}_m^c$ based on large-scale fading $\beta_{m,k}$
3: Estimate $\mathbb{E}\{\mathbf{g}_{ki}^{(m)}\}$, $\mathbb{D}\left\{\mathbf{g}_{ki}^{(m)}\right\}$, and $\mathbb{E}\{\|\mathbf{w}_{m,k}^{\mathrm{H}}\|^2\}$ for every user in $\mathcal{K}_m^c$
4: Upload the statistics of effective channels and $\mathcal{K}_m^c$ to the edge cloud
5: **end parallel**

2) Parallel VSC Selection: The information entropy is increasing when adding more receive antennas [36], which means the increase in the available uplink rate for every user k. Though the rate, achieved by the MMSE-based decoding, has a gap with the information entropy, cooperation reception with more UBSs for every user k can still prompt the SE. In particular, the UBS selection problem is mutually decoupled and independent among different users for the reason that the decoding policy of user k will not influence the others. We define the following discriminant equation $\Psi_k(\mathcal{M}_k, m)$

$$\begin{aligned}\mathbb{E}\left\{\mathbf{g}_{ki}\mathbf{g}_{ki}^{\mathrm{H}}\right\} &\approx \mathbb{E}\left\{\mathbf{g}_{ki}\right\}\mathbb{E}\left\{\mathbf{g}_{ki}^{\mathrm{H}}\right\} - \mathrm{diag}\left\{\mathbb{E}\left\{\mathbf{g}_{ki}\right\}\mathbb{E}\left\{\mathbf{g}_{ki}^{\mathrm{H}}\right\}\right\} + \mathrm{diag}\left\{\mathbb{E}\left\{\mathbf{g}_{ki}\right\}\odot\mathbb{E}\left\{\mathbf{g}_{ki}\right\}\right\} \\ &= \mathbb{E}\left\{\mathbf{g}_{ki}\right\}\mathbb{E}\left\{\mathbf{g}_{ki}^{\mathrm{H}}\right\} - \mathrm{diag}\left\{\left\|\mathbb{E}\left\{\mathbf{g}_{k,i}^{(1)}\right\}\right\|^2, \ldots, \left\|\mathbb{E}\left\{\mathbf{g}_{k,i}^{(|\mathcal{M}_k|)}\right\}\right\|^2\right\} + \mathrm{diag}\left\{\mathbb{E}\left\{\left\|\mathbf{g}_{k,i}^{(1)}\right\|^2\right\}, \ldots, \mathbb{E}\left\{\left\|\mathbf{g}_{k,i}^{(|\mathcal{M}_k|)}\right\|^2\right\}\right\} \\ &= \mathbb{E}\left\{\mathbf{g}_{ki}\right\}\mathbb{E}\left\{\mathbf{g}_{ki}^{\mathrm{H}}\right\} + \mathrm{diag}\left\{\mathbb{D}\left\{\mathbf{g}_{ki}\right\}\right\}\end{aligned} \tag{22}$$

$$\Phi_k\{\mathbf{X}, \boldsymbol{\eta}\} \approx \eta_k\mathbb{E}\left\{\mathbf{g}_{kk}^{\mathrm{H}}\right\}\left(\sum_{i=1, i\neq k}^{K}\eta_i\mathbb{E}\left\{\mathbf{g}_{ki}\right\}\mathbb{E}\left\{\mathbf{g}_{ki}^{\mathrm{H}}\right\} + \sum_{i=1}^{K}\eta_i\mathbf{diag}\left\{\mathbb{D}\left\{\mathbf{g}_{ki}\right\}\right\} + \mathbf{N}_k\right)^{-1}\mathbb{E}\left\{\mathbf{g}_{kk}\right\}. \tag{24}$$

Authorized licensed use limited to: University of Waterloo. Downloaded on August 20,2023 at 10:02:36 UTC from IEEE Xplore. Restrictions apply.

Algorithm 2 SE Maximized VSC Selection

Input: γ_0, $\mathbf{R}_{m,k}$, $m \in \{1,\ldots,M\}, k \in \{1,\ldots,K\}$
$\mathbf{X} = \mathbf{0}$, $\mathbf{Z}$ = Inf (M, K),
$\mathcal{M}_k = \emptyset$, $\mathcal{K}_m = \emptyset$, $\mathcal{Q}_m = \emptyset$
Output: $\mathbf{X}, \mathcal{M}_k, \mathcal{K}_m, k \in \{1,\ldots,K\}$;

parallel for every k in $\mathcal{K}$ **do**:
  Create the candidate service UBS set $\mathcal{M}_k^c$
  for $i = 1; i \le |\mathcal{M}_k^c|; i++$ **do**
    Compute $m = \arg\max_{m, m\in\mathcal{M}_k^c} \Phi_k(\mathcal{M}_k \cup \{m\})$
    if $\Psi(\mathcal{M}_k, m) \ge \gamma_0$ **then**
      if $|\mathcal{K}_m| < \mathcal{K}_T$ **then**
        $\mathcal{M}_k = \mathcal{M}_k \cup \{m\}$
        $\mathcal{K}_m = \mathcal{K}_m \cup \{k\}$
        $\mathbf{Z}(m,k) = \Psi(\mathcal{M}_k, m)$
      else
        $j^* = \arg\min_{j=1,\ldots,K} \mathbf{Z}(m,j)$
        if $\mathbf{Z}(m,j) < \Psi(\mathcal{M}_k, m)$ **then**
          Remove m from $\mathcal{M}_j$
          Remove j from $\mathcal{K}_m$
          $\mathbf{Z}(m,j) = +\infty$
          Run step 3–5
        else
          continue
        end if
      end if
    else
      break
    end if
  end for
  Acquire $x_{m,k}$ according to $\mathcal{M}_k$
end parallel

to determine whether UBS m will serve user k:

$$\Psi_k(\mathcal{M}_k, m) = \frac{\Phi_k(\mathcal{M}_k \cup \{m\}) - \Phi_k(\mathcal{M}_k)}{\Phi_k(\mathcal{M}_k)}, \tag{25}$$

which indicates the marginal effect when adding the UBS m to the VSC of user k. Then, we define the threshold γ_0 for $\Psi(\mathcal{M}, m)$, which implies that only those UBSs whose channel meets the condition $\Psi(\mathcal{M}, m) < \gamma_0$ will serve user k. Next, we propose the SEMVS Algorithm 2, which can be implemented in parallel at the edge cloud.

B. Fractional Programming Based Power Control

As for the NP-hard problem (20a), in this paper, we propose a Lagrangian dual transform [31] in order to tackle the sum logarithmic ratio problems, which moves the SINR term to the outside of logarithm. Recalling the SINR term in (24), we firstly assume

$$\boldsymbol{\mu}_k(\boldsymbol{\eta}) = \boldsymbol{\mu}_k(\hat{\mathbf{X}}, \boldsymbol{\eta}, \boldsymbol{\alpha}^\star) = \sqrt{\eta_k}\mathbb{E}\{\mathbf{g}_{kk}\}, \tag{26}$$

where $\boldsymbol{\mu}_k(\boldsymbol{\eta})$ is a complex vector. In addition, we also assume

$$\mathbf{B}_k = \sum_{i=1, i\neq k}^{K} \eta_i \mathbb{E}\{\mathbf{g}_{ki}\}\mathbb{E}\{\mathbf{g}_{ki}^{\mathrm{H}}\} + \sum_{i=1}^{K} \eta_i \mathbf{diag}\{\mathbb{D}\{\mathbf{g}_{ki}\}\} + \mathbf{N}_k. \tag{27}$$

Then, the weighted sum-of-logarithms maximization object (20a) can be transformed to

$$\max_{\boldsymbol{\eta}} \sum_{k=1}^{K} v_k \log\left(1 + \boldsymbol{\mu}_k^{\mathrm{H}}(\boldsymbol{\eta})\mathbf{B}_k^{-1}(\boldsymbol{\eta})\boldsymbol{\mu}_k(\boldsymbol{\eta})\right) \tag{28a}$$

$$\text{s.t. } 0 \le \eta_k \le \eta_{\max}, \quad \forall\, k \in \mathcal{K}. \tag{28b}$$

where the term $\boldsymbol{\mu}_k^{\mathrm{H}}(\boldsymbol{\eta})\mathbf{B}_k^{-1}(\boldsymbol{\eta})\boldsymbol{\mu}_k(\boldsymbol{\eta})$ can be physically interpreted as the effective SINR term. As for (28a), the following transform is proposed in [29] in order to move the ratio term to the outside of logarithm. For convenience, we denote the object function of (28a) as $\psi(\boldsymbol{\eta}) = \sum_{k=1}^{K} v_k \log\left(1 + \boldsymbol{\mu}_k^{\mathrm{H}}(\boldsymbol{\eta})\mathbf{B}_k^{-1}(\boldsymbol{\eta})\boldsymbol{\mu}_k(\boldsymbol{\eta})\right)$.

Theorem 1 (Lagrangian Dual Transform for Complex Vector): Given a sequence of multidimensional and complex functions $\mu(\eta) : \mathbb{C}^{d_1} \to \mathbb{C}^{d_2}$ for $k \in \mathcal{K}$, a multidimensional function $\mathbf{B}(\eta) : \mathbb{C}^{d_1} \to \mathbb{S}_{++}^{d_2\times d_2}$ and a nonempty constraint set $\boldsymbol{\eta} \in \mathcal{H} \subseteq \mathbb{C}^{d_1}$, where $d_1, d_2 \in \mathbb{N}$, a multidimensional and complex logarithmic FP problem

$$\max_{\boldsymbol{\eta}} \psi(\boldsymbol{\eta}) \quad \text{s.t. } \boldsymbol{\eta} \in \mathcal{H} \tag{29}$$

can be recast to the new expression

$$\max_{\boldsymbol{\eta},\boldsymbol{\gamma}} \mathcal{L}(\boldsymbol{\eta}, \gamma) \quad \text{s.t. } \boldsymbol{\eta} \in \mathcal{H}, \tag{30}$$

in which the new objective function $\mathcal{L}$ is defined as (31), shown at the bottom of the next page, where γ_k is introduced as an auxiliary variable introduced for each SINR term $\boldsymbol{\mu}_k^{\mathrm{H}}(\boldsymbol{\eta})\mathbf{B}_k^{-1}(\boldsymbol{\eta})\boldsymbol{\mu}_k(\boldsymbol{\eta})$. According to [29], the two problems are equivalent for the reason that $\boldsymbol{\eta}$ is the solution to (29) if and only if it is the solution to (30), and the optimal objective values are also equal meanwhile.

Then, applying the Lagrangian dual transform to reformulate the original objective function $\psi(\boldsymbol{\eta})$, we have the new expression $\psi_1(\boldsymbol{\eta}, \boldsymbol{\gamma})$ in (32), shown at the bottom of the next page, where $\boldsymbol{\gamma}$ refers to a collection of auxiliary variables. Now, the ratio terms inside the logarithm function have now been moved outside of the logarithm. Then, accordingly, the original problem (20a) can be expressed as the equivalent optimization problem below

$$\max_{\boldsymbol{\eta},\boldsymbol{\gamma}} \psi_1(\boldsymbol{\eta}, \boldsymbol{\gamma}) \tag{33a}$$

$$\text{s.t. } 0 \le \eta_k \le \eta_{\max}, \quad \forall\, k \in \mathcal{K}. \tag{33b}$$

When $\boldsymbol{\eta}$ are fixed, the optimal can be explicitly determined by setting partial derivative of the Lagrangian

Authorized licensed use limited to: University of Waterloo. Downloaded on August 20,2023 at 10:02:36 UTC from IEEE Xplore. Restrictions apply.

function $\partial\psi_1/\partial\eta_k$ to zero, i.e.,

$$\gamma_i = \eta_k \mathbb{E}\left\{\mathbf{g}_{kk}^{\mathrm{H}}\right\}\left(\sum_{i=1,i\neq k}^{K}\eta_i \mathbb{E}\left\{\mathbf{g}_{ki}\right\}\mathbb{E}\left\{\mathbf{g}_{ki}^{\mathrm{H}}\right\} + \sum_{i=1}^{K}\eta_i \mathrm{diag}\left\{\mathbb{D}\left\{\mathbf{g}_{ki}\right\}\right\} + \mathbf{N}_k\right)^{-1}\mathbb{E}\left\{\mathbf{g}_{kk}\right\}. \quad (34)$$

The optimal γ_k is equal to the effective SINR of user k. Then, in order to decouple the numerators and denominators of the fractional term, the multidimensional and complex quadratic transform is proposed. According to [29], the following theorem holds:

Theorem 2 (Multidimensional and Complex FP): As for $\boldsymbol{\mu}(\boldsymbol{\eta})$ and $\mathbf{B}(\boldsymbol{\eta})$ mentioned above, the original problem

$$\max_{\boldsymbol{\eta}} \ \boldsymbol{\mu}^{\mathrm{H}}(\boldsymbol{\eta})(\mathbf{B}(\boldsymbol{\eta}))^{-1}\boldsymbol{\mu}(\boldsymbol{\eta}) \quad \text{s.t.} \ \ \boldsymbol{\eta}\in\mathcal{H} \quad (35)$$

is equivalent to

$$\max_{\boldsymbol{\eta},\mathbf{y}} \ 2\,\mathrm{Re}\left\{\mathbf{y}^{\mathrm{H}}\boldsymbol{\mu}(\boldsymbol{\eta})\right\} - \mathbf{y}^{\mathrm{H}}\mathbf{B}(\boldsymbol{\eta})\mathbf{y} \quad \text{s.t.} \ \ \boldsymbol{\eta}\in\mathcal{H}, \mathbf{y}\in\mathbb{C}^{d_2}, \quad (36)$$

where $\mathbf{y} = [y_1, \ldots, y_K]$ refers to a collection of auxiliary variables for all users.

In the following, we regard $\sqrt{v_k(1+\gamma_k)\cdot\eta_k}\mathbb{E}\left\{\mathbf{g}_{kk}^{\mathrm{H}}\right\}$ as the numerator term $\boldsymbol{\mu}(\boldsymbol{\eta})$, and regard $\sum_{i=1,i\neq k}^{K}\eta_i\mathbb{E}\left\{\mathbf{g}_{ki}\right\}\mathbb{E}\left\{\mathbf{g}_{ki}^{\mathrm{H}}\right\} + \sum_{i=1}^{K}\eta_i\mathrm{diag}\left\{\mathbb{D}\left\{\mathbf{g}_{ki}\right\}\right\} + \mathbf{N}_k$ as the denominator term $\mathbf{B}(\boldsymbol{\eta})$ in Theorem 2 at the same time. Then, we apply the quadratic transform to the fractional term in (33a) in order to to optimize $\boldsymbol{\eta}$ for fixed $\boldsymbol{\gamma}$. We utilize the Theorem 2 to further reformulate the original object ψ_1 to new object function ψ_2. Then, the new formation of problem (33a) can be denoted as

$$\max_{\boldsymbol{\eta},\boldsymbol{\gamma}} \ \psi_2(\boldsymbol{\eta},\boldsymbol{\gamma},\mathbf{y}) \quad (37a)$$

$$\text{s.t.} \ 0\le\eta_k\le\eta_{\max}, \quad \forall\, k\in\mathcal{K}, \quad (37b)$$

where $\psi_2(\boldsymbol{\eta},\boldsymbol{\gamma},\mathbf{y})$ equals to (38), shown at the bottom of the page.

We propose to maximize $\psi_2(\boldsymbol{\eta},\boldsymbol{\gamma},\mathbf{y})$ over variables $\boldsymbol{\eta},\boldsymbol{\gamma},\mathbf{y}$ in an iterative manner as follows. With the update of γ_k as is shown in (34), we now consider the jointly optimization of $\boldsymbol{\eta}$ and $\mathbf{y}$ in (37a). First, when all the other variables are fixed, the optimal y_k can be explicitly determined by setting $\partial\psi_2/\partial y_k$ to zero, that is

$$\mathbf{y}_k^* = \sqrt{v_k(1+\gamma_k)\eta_k}\cdot\left(\sum_{i=1}^{K}\eta_i\mathbb{E}\left\{\mathbf{g}_{ki}\right\}\mathbb{E}\left\{\mathbf{g}_{ki}^{\mathrm{H}}\right\} + \sum_{i=1}^{K}\eta_i\mathbf{diag}\left\{\mathbb{D}\left\{\mathbf{g}_{ki}\right\}\right\} + \mathbf{N}_k\right)^{-1}\mathbb{E}\left\{\mathbf{g}_{kk}\right\}. \quad (39)$$

Proof 4.1: The details of the proof are shown in Appendix A.

Then, we have the expression of $y_k = (y_k^*)^*$. We can find that the optimal y_k is exactly a minimum mean-square-error (MMSE) receiver scaled by a factor of $\sqrt{v_k(1+\gamma_k)}$ with respect to each user k. Next, if variables $\boldsymbol{\gamma}$ and $\mathbf{y}$ are fixed, we can take the optimal transmission power η_k for user k through solving $\partial\psi_2/\partial\eta_k = 0$. We have

$$\frac{\partial\psi_2}{\partial\eta_k} = \frac{\sqrt{v_k(1+\gamma_k)}\cdot\Re\left\{\mathbb{E}\left\{\mathbf{g}_{kk}^{\mathrm{H}}\right\}y_k\right\}}{\sqrt{\eta_k}} - \sum_{i=1}^{K}y_i^{\mathrm{H}}\mathbb{E}\left\{\mathbf{g}_{ik}\mathbf{g}_{ik}^{\mathrm{H}}\right\}y_i. \quad (40)$$

Then, after settling (40), we have the expression of η_k:

$$\eta_k = \frac{v_k(1+\gamma_k)\cdot\left(\Re\left\{\mathbb{E}\left\{\mathbf{g}_{kk}^{\mathrm{H}}\right\}y_k\right\}\right)^2}{\left(\sum_{i=1}^{K}y_i^{\mathrm{H}}\left(\mathbb{E}\left\{\mathbf{g}_{ik}\right\}\mathbb{E}\left\{\mathbf{g}_{ik}^{\mathrm{H}}\right\} + \mathrm{diag}\left\{\mathbb{D}\left\{\mathbf{g}_{ik}\right\}\right\}\right)y_i\right)^2}. \quad (41)$$

However, every user should be subject to the maximum power constraint, which contributes to the final power

$$\mathcal{L}(\boldsymbol{\eta},\boldsymbol{\gamma}) = \sum_{k=1}^{K}v_k\log(1+\gamma_k) - \sum_{k=1}^{K}v_k\gamma_k + \sum_{k=1}^{K}v_k\cdot(1+\gamma_k)\,\boldsymbol{\mu}_k^{\mathrm{H}}(\boldsymbol{\eta})\left(\boldsymbol{\mu}_k(\boldsymbol{\eta})\boldsymbol{\mu}_k^{\mathrm{H}}(\boldsymbol{\eta}) + \mathbf{B}_k(\boldsymbol{\eta})\right)^{-1}\boldsymbol{\mu}_k(\boldsymbol{\eta}) \quad (31)$$

$$\psi_1(\boldsymbol{\eta},\boldsymbol{\gamma}) = \sum_{k=1}^{K}v_k\left(\log(1+\gamma_k) - \gamma_k + (1+\gamma_k)\cdot\eta_k\mathbb{E}\left\{\mathbf{g}_{kk}^{\mathrm{H}}\right\}\cdot\left(\sum_{i=1}^{K}\eta_i\mathbb{E}\left\{\mathbf{g}_{ki}\right\}\mathbb{E}\left\{\mathbf{g}_{ki}^{\mathrm{H}}\right\} + \sum_{i=1}^{K}\eta_i\mathbf{diag}\left\{\mathbb{D}\left\{\mathbf{g}_{ki}\right\}\right\} + \mathbf{N}_k\right)^{-1}\mathbb{E}\left\{\mathbf{g}_{kk}\right\}\right) \quad (32)$$

$$\psi_2(\boldsymbol{\eta},\boldsymbol{\gamma},\mathbf{y}) = \sum_{k=1}^{K}v_k\log(1+\gamma_k) - \sum_{k=1}^{K}v_k\gamma_k + \sum_{k=1}^{K}\left(2\sqrt{v_k(1+\gamma_k)\eta_k}\Re\left\{\mathbb{E}\{\mathbf{g}_{kk}^{\mathrm{H}}\}y_k\right\} - y_k^{\mathrm{H}}\left(\sum_{i=1}^{K}\eta_i\mathbb{E}\left\{\mathbf{g}_{ki}\right\}\mathbb{E}\left\{\mathbf{g}_{ki}^{\mathrm{H}}\right\} + \sum_{i=1}^{K}\eta_i\mathbf{diag}\left\{\mathbb{D}\left\{\mathbf{g}_{ki}\right\}\right\} + \mathbf{N}_k\right)\mathbf{y}_k\right). \quad (38)$$

Authorized licensed use limited to: University of Waterloo. Downloaded on August 20,2023 at 10:02:36 UTC from IEEE Xplore. Restrictions apply.

control decision

$$\eta_k^{\star} = \min\left\{\eta_{\max}, \eta_k^{\star}\right\}. \tag{42}$$

Then, according to (39), (34) and (42), we propose to maximize ψ_2 for variables $\mathbf{y}$, γ, and $\boldsymbol{\eta}$ in an iterative manner as shown in the Algorithm 3:

Algorithm 3 Proposed Matrix Fractional Programming Strategy for Uplink Power Control

Input: Initialize all variables to feasible values: $\hat{\mathbf{y}}, \hat{\boldsymbol{\eta}}, \hat{\boldsymbol{\gamma}}, \mathcal{I}_{\max}$, ϵ, $\mathrm{i} = 0$

Output: Users' transmission power: $\hat{\boldsymbol{\eta}}$

1: **repeat**
2: Update $\hat{\mathbf{y}}^{(i+1)}$ according to (39) and (34)
3: Update $\hat{\boldsymbol{\gamma}}^{(i+1)}$ according to (34)
4: Update $\hat{\eta}^{(i+1)}$ according to (41) and (42)
5: **until** the weighted sum-rate converges.
6: **return** $\hat{\boldsymbol{\eta}}$;

V. Numerical Results and Discussions

A. Simulation Setup

We consider a scenario with 1 control BS, $M = 64$ UBSs with antennas $N = 4$, and $K = 30$ users distributed in a $1000m \times 1000m$ square area. All the UBSs and users are independently and uniformly in the area of interest. Utilizing the distance-based wrap-around simulation strategy [37], we can acquire the performance of the network with 30 active users/km^2 and 256 antennas/km^2. In this area, all UBSs receive both signal and interference from all directions simultaneously. As for m-MIMO cellular network (Cellular), we keep the same number of antennas with $M_c = 4$ BSs and $N_c = 64$ antennas in the same area. And, we also consider the small cell scenario, in which $M_s = 64$ small cells, each with $N_s = 4$ antennas, are uniformly distributed in the same area. Besides, we assume that the channel follows spatially correlated Rayleigh fading [15] at 2 GHz carrier frequency, where the large-scale fading is based on the 3GPP Standards [37] and the spatial correlation matrices is generated employing [15]. We assume $\tau_c = 200$, $\tau_p = 10$, which corresponding to the case of 2 ms correlation time and 100 kHz coherence bandwidth. In addition, we assume that the transmit power is up to 200 mW with a bandwidth 20 MHz, and the noise power spectrum density is -174 dBm/Hz with a noise figure 7 dB. In this paper, the computation of EE is according to [38] and [39], which is detailly described in the Appendix B. Here, we choose the following parameters: $P_U = 0.1$ W, $P_{\text{fix}} = 0.825$ W. For the cellular network, the fixed power consumption (control signals, backhaul, etc.) P_{fix} is assumed to be 18 W. Also, the traffic-dependent fronthaul power is $0.25\,W/(Gbits/s)$, and the maximum transmit power is 0.2 W for all users.

In the following, we first compare diverse performance benchmarks between SEMVS-based FD-RAN and other networks, namely m-MIMO cellular network, small cell, LSFD-based cell-free network (LSCF) [15], and LSFD-based cell-free network with the Dynamic Cooperation Clustering (DCC-LSCF) [15]. Then, we compare the proposed FPPC power control algorithm with several state-of-the-art algorithms. At last, we further investigate the relationship between the m-MIMO cellular network and the number of UBSs.

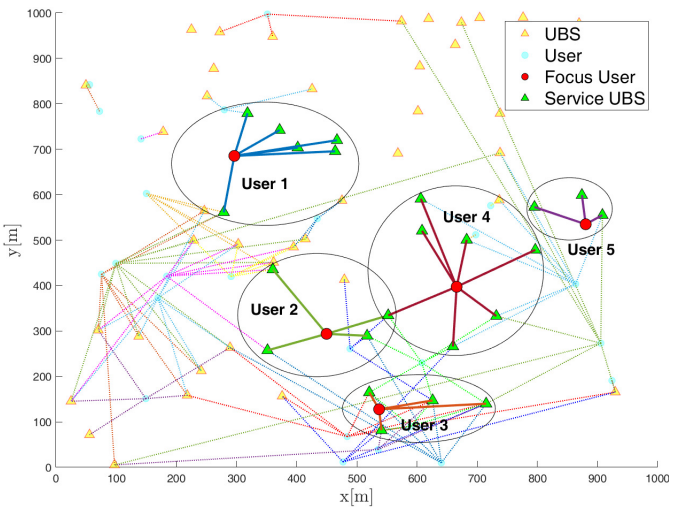

Fig. 2. Distribution of users and UBS, and VSCs for partial users.

B. Virtual Service Clustering

In order to clearly show the association between users and UBSs, we validate the Wrap policy temporarily in this subsection. Fig. 2 illustrates the virtual service clusters for partial users in FD-RAN, which is achieved by the proposed SEMVS. In Fig. 2, service UBSs for users are connected with semi-transparent lines. Specifically, we strengthen some users with circle dashed lines, whose service UBSs are clear to observe. It is obvious that service UBSs for each user will come into being a VSC. With the unified control of VSC, the virtual association in FD-RAN is extremely flexible and dynamic with users' movements as time goes on. That is, users will enjoy a continuous and handover-imperceptible service, which is almost impossible to achieve in traditional cellular networks.

C. Spectrum Efficiency

As illustrated in Fig. 3(a), the performance of FD-RAN with SEMVS algorithm is far superior to that of m-MIMO cellular networks, especially for those users undergoing poor channel (small window area). Compared to the LSCF and DCC-LSCF in [16], the proposed SEMVS algorithm holds almost the same cumulative distribution function (CDF) for the SE, which is on the condition that FD-RAN only employs approximate one-fifth of the average number of UBSs compared to DCC-LSCF. Besides, the FD-RAN still has a large SE improvement compared to the small cell for the users with poor channels, which shows the superiority in cooperation reception. By comparing the different scenarios, we notice that the users with poor channel conditions experience lower SE in the m-MIMO network, since there are larger location gaps between those users and BSs compared to FD-RAN. On the

Authorized licensed use limited to: University of Waterloo. Downloaded on August 20,2023 at 10:02:36 UTC from IEEE Xplore. Restrictions apply.

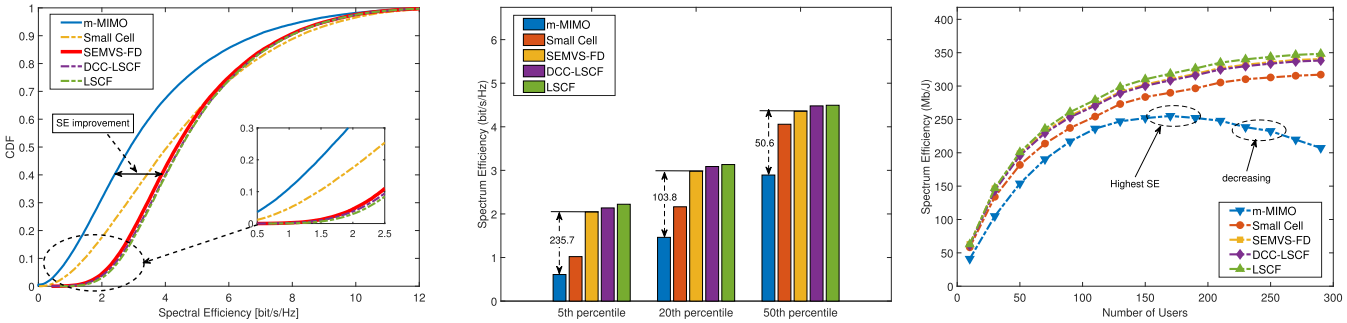

(a) The CDF of each user's SE for different architectures.

(b) The comparison of SE for 5th, 20th, and 50th percentile.

(c) The comparison of SE with the increasing number of users.

Fig. 3. SE comparison among different network architectures.

contrary, as shown in Fig. 3a, users in FD-RAN with ideal channel conditions will have about the same SE as those in an m-MIMO network. It might be the reason that these users are sensitive to interference and each UBS can locally suppress interference using its array of antennas, and the cooperation of multiple UBSs makes up for the weakness of fewer BSs. Therefore, the proposed FD-RAN is capable of suppressing mutual interference so that everyone can transmit at maximum power.

Specifically, we can notice Fig. 3(b) that the FD-RAN accompanied with SEMVS can achieve nearly 235.7% SE improvement for the 5th percentile user when compared to that of the cellular network. Furthermore, the 20th and 50th percentile users in FD-RAN still demonstrate a 103.8% and 50% SE improvement than that in the cellular network, respectively. The percentile results further validate the fact that the FD-RAN will bring better performance improvement to users with poor channel conditions.

Fig. 3(c) shows that the SE of FD-RAN is always increasing. This is because the MMSE-driven two-layer combination framework can compress interference among different users, and the smaller average distance between users and UBSs will enhance the effectiveness of SINR. On the contrary, the SE of both the m-MIMO network and the small cell will decrease when the load is heavy with increasing users. With respect to m-MIMO, a single BS typically serves several times more users than FD-RAN, and the increasing average distance between the user and BS will lead to a poor channel for more users who are far away from the BS. This causes severe inter-user interference, i.e., low SINR. In terms of small cell, a single BS with only a few antennas has limited interference suppression, but FD-RAN might utilize the collaboration of several BSs through the 2nd layer combination. Interestingly, the SE performance in SEMVS-FD even exceeds that in DCC-LSCF sometimes, which might be the reason that the SEMVS algorithm forms a more appropriate VSC.

D. Energy Efficiency

In Fig. 4(a), we can notice that the EE of the proposed algorithm is much higher than m-MIMO and LSCF network, and the performance improvements reach 70.1% and 55.3% separately. Then, the FD-RAN still has a EE improvement of 12.8% compared to the DCC-LSCF. Furthermore, the EE in FD-RAN is even superior to small cell network in which every user employs only one BSs, though the EE in DCC-LSCF is lower than small cell. Because the fronthaul load in SEMVS is much smaller than that in DCC, which in turn leads to lower fronthaul cost.

Moreover, we compare the EE with different network service users in Fig. 4(b). We find that the EE in FD-RAN has 95.4%, 54.3%, and 35% improvements compared to m-MIMO when there are 10, 50, and 90 users respectively. Besides, there are still 28.4%, 64.6%, and 64.3% EE improvements between the FD-RAN and LSCF for 10, 50, and 90 service users, respectively.

Then, we observe the EE change for increasing users further. In Fig. 4(c), we find that the EE of the FD-RAN is always superior to other schemes. Generally, the EE of all the schemes will firstly increase until the highest EE, and then decrease according to the increase of users. The differences are the value of the highest EE and the number of users when achieving it. As for FD-RAN, DCC-LSCF, and small cell, it will approach the highest EE when the number of users is approximate to the number of UBSs/APs (64). However, it will approach the highest EE for LSCF when the number of users is smaller (60), which might be the reason for the high power consumption of the fronthaul. There are two cross points P1 and P2 for LSCF and m-MIMO. As for the P1, the fast-increasing fronthaul consumption will offset the gain of SE improvements for LSCF. As for the P2, the SE of m-MIMO will rapidly decline for strong interference when the network load becomes heavier.

E. VSC and Fronthaul Load

Fig. 5(a) depicts the distribution of the size of VSC for SEMVS and DCC. We find that the distribution of VSC sizes produced by these two algorithms differed significantly, with SEMVS being much smaller than DCC and more uniformly distributed, which would lead to different calculations and energy costs (Fig. 4). As represented in Fig. 5(b), compared with the DCC, the average fronthaul load of SEMVS (2.1 users/UBS) is much smaller than that in DCC [15] (9.3users/BS). Moreover, we can observe that the VSC size (average virtual service UBSs) for every

Authorized licensed use limited to: University of Waterloo. Downloaded on August 20,2023 at 10:02:36 UTC from IEEE Xplore. Restrictions apply.

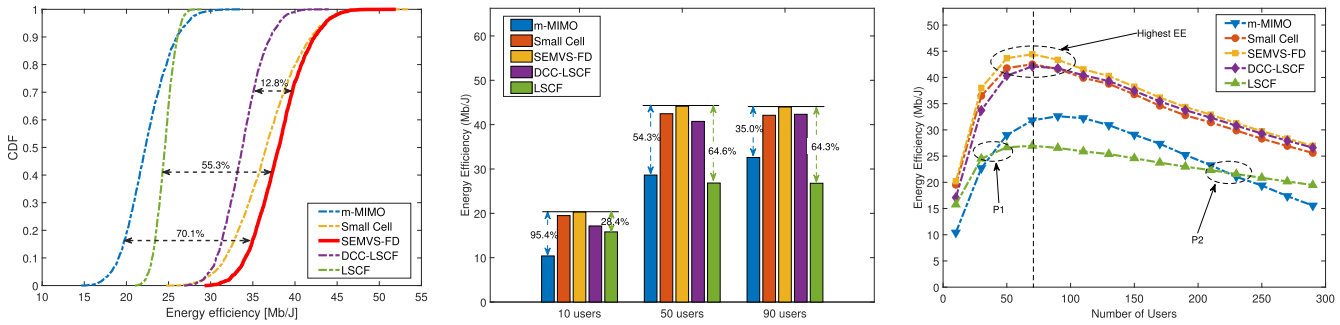

(a) The CDF of each user's EE for different architectures.

(b) The comparison of EE for 10, 50, 90 users.

(c) The comparison of EE with the increasing number of users.

Fig. 4. EE comparison among different network architectures.

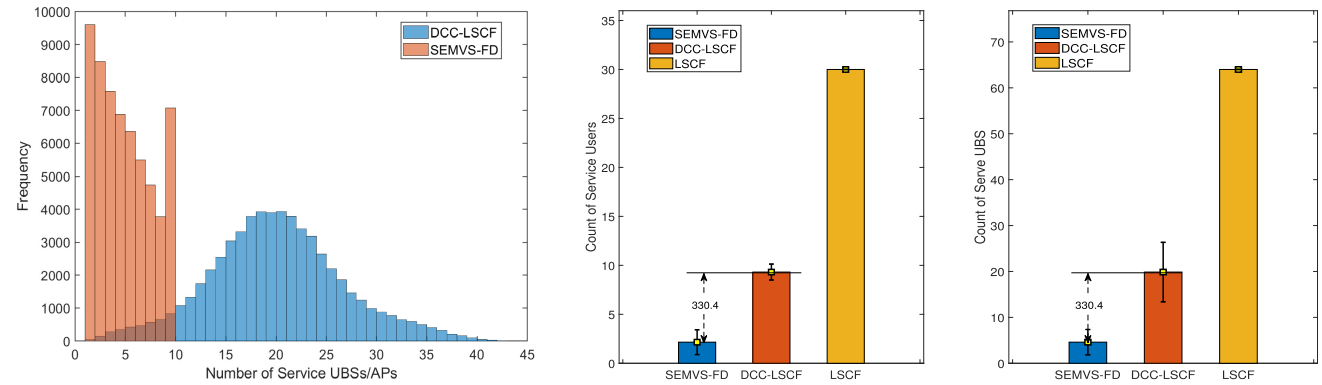

(a) Distribution of the size of VSC.

(b) Average Fronthaul.

(c) Average size of VSC.

Fig. 5. Comparison of fronthaul and number of service UBSs for different algorithms.

user in SEMVS (4.6 UBSs/user) is also much smaller than DCC (19.9 UBSs/user), which is shown in Fig. 5(c). According to the phenomenon above mentioned, the VSC size will directly affect the EE of the network, while adding an extra UBS to the VSC might result in negligible SE improvement. From this point of view, the proposed SEMVS can achieve a better balance between SE and EE.

F. Uplink Power Control

As for the uplink transmit power control, we emphatically compare the proposed FPPC algorithm with WMMSE and other three heuristic but scalable benchmarks schemes:

- WMMSE. The WMMSE algorithm has been well studied in the literature as a beamforming scheme, and adaptive power control is implicitly included in the uplink power control [16].
- Fractional Power Control (FPC). We consider the fractional power control scheme with exponents [30], [40].
- Full Power. All users transmit with full power.

1) Spectrum Efficiency: Fig. 6 compares the uplink SE of the power control methods described above. We can obviously observe that no matter what the network load is, the proposed FPPC algorithm always achieves the highest SE. When the network load is light, almost all the algorithms mentioned have the same SE. However. Compared to the full power transmission, the improvements of FPPC will become more obvious (6% for 190 users) as the network load increases.

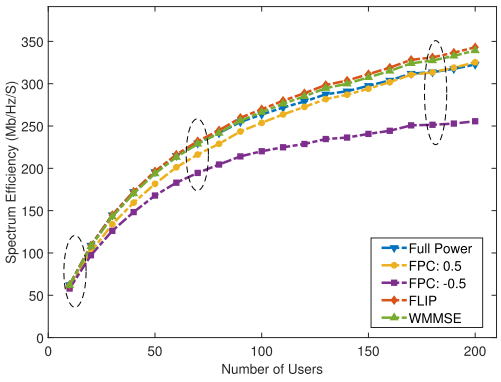

Fig. 6. SE with the increasing number of users for different power control algorithms.

This is because network interference is becoming serious and affects the decoding when the network is under a heavy load. In addition, the sum SE maximizing power control algorithms, namely WMMSE and FPPC, provide almost the same SE performance.

2) Energy Efficiency: In Fig. 7, we can view the uplink EE with increasing users. At a first glance, when the network has a small load, all the algorithms have a similar EE, because almost all the users transmit with full power at this moment. As the service users increase, the EE of the full-power version will decrease rapidly, but the EE of FPPC and WMMSE still slowly increase. It's the reason that the speed of SE

Authorized licensed use limited to: University of Waterloo. Downloaded on August 20,2023 at 10:02:36 UTC from IEEE Xplore. Restrictions apply.

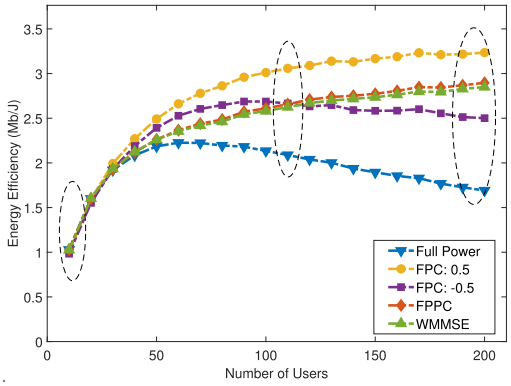

Fig. 7. EE with the increasing number of users for different power control algorithms.

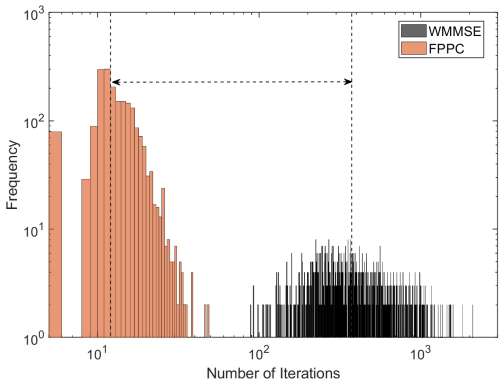

Fig. 8. Comparison of iteration number between WMMSE and FPPC.

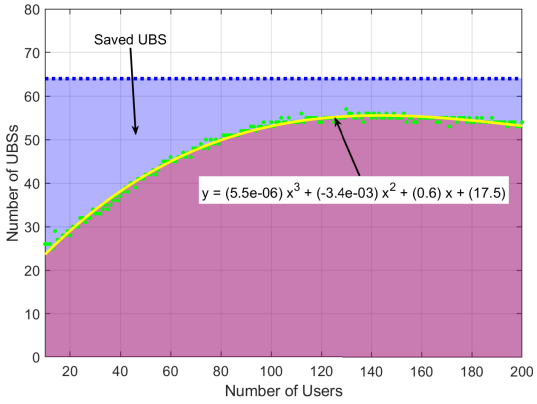

Fig. 9. Comparison of UBS number when achieving the same SE.

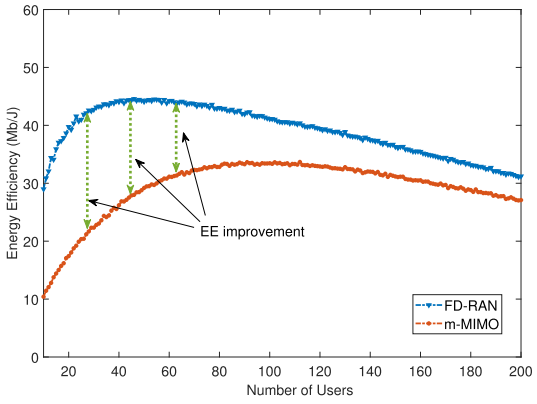

Fig. 10. Comparison of EE when achieving the same SE.

increasing in full power schema is slower than that of total power consumption. The EE of FPPC is lower than the FPC with the exponent equaling 0.5, but the high EE of FPC is at cost of lower SE. Moreover, the EE of FPC with the exponent equaling 0.5 and -0.5 has completely different SE and EE, which means that the selection of exponent parameters is crucial in this schema, and leads to diverse performance. In addition, the FPPC algorithm has a higher but still negligible EE compared with the WMMSE. Considering the same situation for SE, it reveals that the similar iteration algorithms, FPPC and WMMSE, wouldn't lead to great discrimination in SE and EE performance. At this time, the iteration number will play a vital factor in power control.

3) Iterations: In Fig. 8, we show the distribution of iteration number of FPPC and WMMSE, where both the x-axis and y-axis are in a log manner. We can find that the FPPC algorithm can terminate the operation within 50 iterations for most scenarios. However, the WMMSE will terminate for a mean iteration number of 500, which is a gap over an order of magnitude. Specifically, there are some scenarios where the process will terminate within one iteration. Because, users will tend to transmit with full power when the interference is low, which makes the transmit powers of all users approximate or exceed the maximum power at the first iteration. Given the approximate SE and EE, the proposed FPPC is more computation-efficient than the WMMSE algorithm from the perspective of iteration number.

G. Comparison Between FD-RAN and m-MIMO When Achieving the Same SE

Fig. 9 demonstrates how many UBSs can achieve greater SE than 4 m-MIMO BSs with 64 antennas when the number of users varies. And, the green dots represent corresponding UBSs counts. We find the data can be fitted into a three-order polynomial, and the yellow curve represents the final results. It is noteworthy that the curve will first rise and then decline as the number of service users increases. This is identical to the m-MIMO SE trend depicted in Fig. 3(c). When the number of UBS is 57, Fig. 9 indicates that the uplink SE of FD-RAN is always greater than that of m-MIMO. Additionally, when the network load is low (less than 20 active users), FD-RAN can achieve the same SE with half as many antennas (32 UBSs) as m-MIMO. Even if the network is in heavy load (60 active users), FD-RAN only requires 70% as many antennas as m-MIMO. The top blue line means that there are 64 UBSs with 4 antennas, indicating that FD-RAN and m-MIMO networks have the same number of antennas (256 antennas). Then, the purple area means how many of UBSs can be saved when the same number of users is served by FD-RAN. To some extent, this figure can provide some guidance on the deployment of the FD-RAN uplink network when achieving the same SE as m-MIMO under a specific network load.

Then, in Fig. 10, we compare the EE of FD-RAN and m-MIMO when they achieve the same SE. We can find that the EE in FD-RAN is far greater than that in m-MIMO,

Authorized licensed use limited to: University of Waterloo. Downloaded on August 20,2023 at 10:02:36 UTC from IEEE Xplore. Restrictions apply.

especially when the network load is low. In particular, the EE improvements respectively reach 178.5%, 128.0%, and 91.2% when the network has 10, 20, and 30 active users to be served. And, the EE still has more than 40% improvement when the network load is heavy (60 active users). It means that the FD-RAN will possess far better EE than m-MIMO when they have the same SE.

VI. Conclusion

We have investigated a resilient uplink base stations cooperative reception framework in FD-RAN. Firstly, we have proposed a two-tier signal combination approach and formulated the UBSs selection as an effective spectrum efficiency maximization problem. And, we have developed a VSC selection algorithm for the flexible service subset scheduling. Then, the FPPC algorithm has been proposed for efficient user power control, which can hold a higher SE compared to the other schemes, and provide a balance between SE and EE. In addition, by completely decoupling the traditional base station, the FD-RAN can implement extremely flexible network resources management and cooperation, which shed light on the new perspective, namely shifting the attention from single BS performance to network-level performance in terms of SE and EE. In our future work, we will investigate switching on/off the UBSs to achieve more energy efficiency communications. Furthermore, the on-demand deployment of UBSs and DBSs will also be an important issue in balancing QoS assurance and cost/power consumption in future networks.

Appendix A
Proof of Theorem 1

We define the complex variable: $z = x+i\cdot y \in C$, in which x is the real part. Then, according to [41], we have the following conclusion:

$$\frac{\partial}{\partial z} = \frac{1}{2}\cdot\left(\frac{\partial}{\partial x} - i\cdot\frac{\partial}{\partial y}\right)$$

Let complex vector $\mathbf{z} \in \mathbb{C}^{M\times 1}$, and complex matrix $\mathbf{B} \in \mathbb{C}^{M\times M}$. $\mathbf{B}_{\mathrm{R}}$ and $\mathbf{z}_{\mathrm{R}}$ denote the real parts of $\mathbf{B}$ and $\mathbf{z}$ while $\mathbf{B}_{\mathrm{I}}, \mathbf{z}_{\mathrm{I}}$ denote the image parts. Then, $\mathbf{B}^{\mathrm{H}}\mathbf{z}$ can be reformatted to

$$\mathbf{B}^{\mathrm{H}}\mathbf{z} = (\mathbf{B}_{\mathrm{R}} + i\cdot\mathbf{B}_{\mathrm{I}})^{\mathrm{H}}(\mathbf{z}_{\mathrm{R}} + i\cdot\mathbf{z}_{\mathrm{I}}) \tag{43}$$

where the real part is $\Re(\mathbf{B}^{\mathrm{H}}\mathbf{z}) = \mathbf{B}_{\mathrm{R}}^{\mathrm{T}}\mathbf{z}_{\mathrm{R}} - \mathbf{B}_{\mathrm{I}}^{\mathrm{T}}\mathbf{z}_{\mathrm{I}}$. Then, we have the derivative of the real part of $\mathbf{B}^{\mathrm{H}}\mathbf{z}$ with respect to $\mathbf{z}$:

$$\begin{aligned}\frac{\partial\Re(\mathbf{B}^{\mathrm{H}}\mathbf{z})}{\partial\mathbf{z}} &= \frac{1}{2}\cdot\left(\frac{\partial\Re(\mathbf{B}^{\mathrm{H}}\mathbf{z})}{\partial\mathbf{z}_{\mathrm{R}}} - i\cdot\frac{\partial\Re(\mathbf{B}^{\mathrm{H}}\mathbf{z})}{\partial\mathbf{z}_{\mathrm{I}}}\right)\\ &= \frac{1}{2}\cdot\left(\frac{\partial\mathbf{B}_{\mathrm{R}}^{\mathrm{T}}\mathbf{z}_{\mathrm{R}} - \mathbf{B}_{\mathrm{I}}^{\mathrm{T}}\mathbf{z}_{\mathrm{I}}}{\partial\mathbf{z}_{\mathrm{R}}} - i\cdot\frac{\partial\mathbf{B}_{\mathrm{R}}^{\mathrm{T}}\mathbf{z}_{\mathrm{R}} - \mathbf{B}_{\mathrm{I}}^{\mathrm{T}}\mathbf{z}_{\mathrm{I}}}{\partial\mathbf{z}_{\mathrm{I}}}\right)\\ &= \frac{1}{2}\cdot(\mathbf{B}_R + i\cdot\mathbf{B}_{\mathrm{I}}) = \frac{1}{2}\cdot\mathbf{B}\end{aligned} \tag{44}$$

For the reason that $\mathbf{B}$ is Hermitian, the complex quadratic form $\mathbf{z}^{\mathrm{H}}\mathbf{B}\mathbf{z}$ can be expanded into

$$\begin{aligned}\mathbf{z}^{\mathrm{H}}\mathbf{B}\mathbf{z} &= (\mathbf{z}_{\mathrm{R}} + i\cdot\mathbf{z}_{\mathrm{I}})^{\mathrm{H}}(\mathbf{B}_{\mathrm{R}} + i\cdot\mathbf{B}_{\mathrm{I}})(\mathbf{z}_{\mathrm{R}} + i\cdot\mathbf{z}_{\mathrm{I}})\\ &= \mathbf{z}_{\mathrm{R}}^{\mathrm{T}}\mathbf{B}_{\mathrm{R}}\mathbf{z}_{\mathrm{R}} - \mathbf{z}_{\mathrm{R}}^{\mathrm{T}}\mathbf{B}_{\mathrm{I}}\mathbf{z}_{\mathrm{I}} + \mathbf{z}_{\mathrm{I}}^{\mathrm{T}}\mathbf{B}_{\mathrm{R}}\mathbf{z}_{\mathrm{I}} + \mathbf{z}_{\mathrm{I}}^{\mathrm{T}}\mathbf{B}_{\mathrm{I}}\mathbf{z}_{\mathrm{R}}\end{aligned} \tag{45}$$

According to the properties of the Hermitian matrix, $\mathbf{B}_{\mathrm{R}}^{\mathrm{T}} = \mathbf{B}_R$, $\mathbf{B}_{\mathrm{I}}^{\mathrm{T}} = -\mathbf{B}_{\mathrm{I}}$, Therefore, we have the following inference:

$$\begin{aligned}\frac{\partial\mathbf{z}^{\mathrm{H}}\mathbf{B}\mathbf{z}}{\partial\mathbf{z}} &= \frac{1}{2}\cdot\left(\frac{\partial\mathbf{z}^{\mathrm{H}}\mathbf{B}\mathbf{z}}{\partial\mathbf{z}_{\mathrm{R}}} - i\cdot\frac{\partial\mathbf{z}^{\mathrm{H}}\mathbf{B}\mathbf{z}}{\partial\mathbf{z}_{\mathrm{I}}}\right)\\ &= \frac{1}{2}\cdot[2\mathbf{B}_{\mathrm{R}}\mathbf{z}_{\mathrm{R}} - 2\mathbf{B}_{\mathrm{I}}\mathbf{z}_{\mathrm{I}} - i\cdot(2\mathbf{B}_{\mathrm{I}}\mathbf{z}_{\mathrm{R}} + 2\mathbf{B}_{\mathrm{R}}\mathbf{z}_{\mathrm{I}})]\\ &= \left(\mathbf{B}_{\mathrm{R}}^{\mathrm{T}} + i\cdot\mathbf{B}_{\mathrm{I}}^{\mathrm{T}}\right)(\mathbf{z}_{\mathrm{R}} - i\cdot\mathbf{z}_{\mathrm{I}}) = \mathbf{B}^T\mathbf{z}^*\end{aligned} \tag{46}$$

Therefore, applying inference (44) and (46) to (38), we have the partial derivative of $\partial\psi_2/\partial y_k$:

$$\begin{aligned}\frac{\partial\psi_2}{\partial y_k} = &\sqrt{v_k(1+\gamma_k)\eta_k}\cdot\mathbb{E}\{\mathbf{g}_{kk}\}\\ &-\left(\sum_{i=1}^{K}\eta_i\mathbb{E}\left\{\mathbf{g}_{ki}\mathbf{g}_{ki}^{\mathrm{H}}\right\} + \mathbf{N}_k\right)^{\mathrm{T}} y_k^*\end{aligned} \tag{47}$$

Then, we can acquire the expression of y_k in (39).

Appendix B
Energy Efficiency

The total uplink power consumption can be defined as follows:

$$P_{\text{total}} = P_{\mathrm{TX}} + P_{\mathrm{CP}} \tag{48}$$

where P_{TX} is the uplink power amplifiers (PAs) due to transmit power at the users and PA dissipation, and P_{CP} refers to the circuit power (CP) consumption. The power consumption P_{TX} is given by $P_{\mathrm{TX}} = \frac{1}{\zeta}\sum_{k=1}^{K}\eta_k$, where ζ is the PA efficiency at each user. The power consumption P_{CP} is obtained as

$$P_{\mathrm{CP}} = MP_{\mathrm{fix}} + KP_{\mathrm{U}} + \sum_{m=1}^{M}P_{\mathrm{fh},m}, \tag{49}$$

where P_{fix} is a fixed power consumption (including control signals and fronthaul) at each UBS/AP, PU denotes the required power to run circuit components at each user and finally, fronthaul power consumption from the m_{th} UBS/AP to the CPU is obtained as follows

$$P_{\mathrm{fh},m} = R_{\mathrm{fh},m}C_{\mathrm{th}} \tag{50}$$

where C_{th} is the fronthaul traffic (BT) between the m_{th} UBS/AP and the CPU, while $P_{\mathrm{BT},m}$ means the corresponding unit power consumption for fronthaul. Then, we formulate the total EE of the FD-RAN uplink network. The total EE is achieved by dividing the sum throughput by the total consumed power, which is given by

$$E_e(\mathbf{X}, \boldsymbol{\eta}, \boldsymbol{\alpha}^\star) = \frac{B\cdot\hat{\Phi}\{\mathbf{X}, \boldsymbol{\eta}, \boldsymbol{\alpha}^\star\}}{P_{\text{total}}}\left(\frac{\text{bit}}{\text{Joule}}\right) \tag{51}$$

References

[1] W. Saad, M. Bennis, and M. Chen, "A vision of 6G wireless systems: Applications, trends, technologies, and open research problems," *IEEE Netw.*, vol. 34, no. 3, pp. 134–142, Jun. 2019.

[2] Q. Yu et al., "A fully-decoupled RAN architecture for 6G inspired by neurotransmission," *J. Commun. Inf. Netw.*, vol. 4, no. 4, pp. 15–23, Dec. 2019.

Authorized licensed use limited to: University of Waterloo. Downloaded on August 20,2023 at 10:02:36 UTC from IEEE Xplore. Restrictions apply.

[3] X. Shen, J. Gao, W. Wu, M. Li, C. Zhou, and W. Zhuang, "Holistic network virtualization and pervasive network intelligence for 6G," *IEEE Commun. Surveys Tuts.*, vol. 24, no. 1, pp. 1–30, 1st Quart., 2022.

[4] M. Giordani, M. Polese, M. Mezzavilla, S. Rangan, and M. Zorzi, "Toward 6G networks: Use cases and technologies," *IEEE Commun. Mag.*, vol. 58, no. 3, pp. 55–61, Mar. 2020.

[5] W. Wu et al., "AI-native network slicing for 6G networks," *IEEE Wireless Commun.*, vol. 29, no. 1, pp. 96–103, Feb. 2022.

[6] H. Zhou, W. Xu, Y. Bi, J. Chen, Q. Yu, and X. S. Shen, "Toward 5G spectrum sharing for immersive-experience-driven vehicular communications," *IEEE Wireless Commun.*, vol. 24, no. 6, pp. 30–37, Dec. 2017.

[7] N. Kato et al., "Optimizing space-air-ground integrated networks by artificial intelligence," *IEEE Wireless Commun.*, vol. 26, no. 4, pp. 140–147, Aug. 2019.

[8] H. Guo, J. Li, J. Liu, N. Tian, and N. Kato, "A survey on space-air-ground-sea integrated network security in 6G," *IEEE Commun. Surveys Tuts.*, vol. 24, no. 1, pp. 53–87, 1st Quart., 2022.

[9] K. B. Letaief and W. Zhang, "Cooperative communications for cognitive radio networks," *Proc. IEEE*, vol. 97, no. 5, pp. 878–893, May 2009.

[10] K. Hamdi, W. Zhang, and K. B. Letaief, "Opportunistic spectrum sharing in cognitive MIMO wireless networks," *IEEE Trans. Wireless Commun.*, vol. 8, no. 8, pp. 4098–4109, Aug. 2009.

[11] E. Nayebi, A. Ashikhmin, T. L. Marzetta, and B. D. Rao, "Performance of cell-free massive MIMO systems with MMSE and LSFD receivers," in *Proc. 50th Asilomar Conf. Signals, Syst. Comput.*, Nov. 2016, pp. 203–207.

[12] A. Checko et al., "Cloud RAN for mobile networks-A technology overview," *IEEE Commun. Surveys Tuts.*, vol. 17, no. 1, pp. 405–426, 1st Quart., 2015.

[13] R. Heath, S. Peters, Y. Wang, and J. Zhang, "A current perspective on distributed antenna systems for the downlink of cellular systems," *IEEE Commun. Mag.*, vol. 51, no. 4, pp. 161–167, Apr. 2013.

[14] H. Q. Ngo, A. Ashikhmin, H. Yang, E. G. Larsson, and T. L. Marzetta, "Cell-free massive MIMO versus small cells," *IEEE Trans. Wireless Commun.*, vol. 16, no. 3, pp. 1834–1850, Mar. 2017.

[15] E. Björnson and L. Sanguinetti, "Making cell-free massive MIMO competitive with MMSE processing and centralized implementation," *IEEE Trans. Wireless Commun.*, vol. 19, no. 1, pp. 77–90, Jan. 2020.

[16] O. T. Demir, E. Bjornson, and L. Sanguinetti, "Foundations of user-centric cell-free massive MIMO," *Found. Trends Signal Process.*, vol. 14, nos. 3–4, pp. 162–472, 2021.

[17] T. L. Marzetta, *Fundamentals Massive MIMO*. Cambridge, U.K.: Cambridge Univ. Press, 2016.

[18] M. Bashar et al., "Exploiting deep learning in limited-fronthaul cell-free massive MIMO uplink," *IEEE J. Sel. Areas Commun.*, vol. 38, no. 8, pp. 1678–1697, Aug. 2020.

[19] H. Masoumi and M. J. Emadi, "Performance analysis of cell-free massive MIMO system with limited fronthaul capacity and hardware impairments," *IEEE Trans. Wireless Commun.*, vol. 19, no. 2, pp. 1038–1053, Feb. 2019.

[20] G. Femenias and F. Riera-Palou, "Cell-free millimeter-wave massive MIMO systems with limited fronthaul capacity," *IEEE Access*, vol. 7, pp. 44596–44612, 2019.

[21] G. Interdonato, E. Björnson, H. Quoc Ngo, P. Frenger, and E. G. Larsson, "Ubiquitous cell-free massive MIMO communications," *EURASIP J. Wireless Commun. Netw.*, vol. 2019, no. 1, pp. 1–13, Dec. 2019.

[22] S. Zaidi, O. B. Smida, S. Affes, U. Vilaipornsawai, L. Zhang, and P. Zhu, "User-centric base-station wireless access virtualization for future 5G networks," *IEEE Trans. Commun.*, vol. 67, no. 7, pp. 5190–5202, Jul. 2019.

[23] M. Guenach, A. A. Gorji, and A. Bourdoux, "Joint power control and access point scheduling in fronthaul-constrained uplink cell-free massive MIMO systems," *IEEE Trans. Commun.*, vol. 69, no. 4, pp. 2709–2722, Apr. 2021.

[24] M. Bashar, K. Cumanan, A. G. Burr, H. Q. Ngo, M. Debbah, and P. Xiao, "Max–min rate of cell-free massive MIMO uplink with optimal uniform quantization," *IEEE Trans. Commun.*, vol. 67, no. 10, pp. 6796–6815, Oct. 2019.

[25] M. Bashar, K. Cumanan, A. G. Burr, M. Debbah, and H. Q. Ngo, "On the uplink max-min SINR of cell-free massive MIMO systems," *IEEE Trans. Wireless Commun.*, vol. 18, no. 4, pp. 2021–2036, Apr. 2019.

[26] L. Liu, R. Zhang, and K.-C. Chua, "Achieving global optimality for weighted sum-rate maximization in the K-user Gaussian interference channel with multiple antennas," *IEEE Trans. Wireless Commun.*, vol. 11, no. 5, pp. 1933–1945, May 2012.

[27] E. Björnson and E. Jorswieck, "Optimal resource allocation in coordinated multi-cell systems," *Found. Trends Commun. Inf. Theory*, vol. 9, nos. 2–3, pp. 113–381, 2013.

[28] W. Utschick and J. Brehmer, "Monotonic optimization framework for coordinated beamforming in multicell networks," *IEEE Trans. Signal Process.*, vol. 60, no. 4, pp. 1899–1909, Apr. 2012.

[29] K. Shen and W. Yu, "Fractional programming for communication systems—Part I: Power control and beamforming," *IEEE Trans. Signal Process.*, vol. 66, no. 10, pp. 2616–2630, May 2018.

[30] Q. Shi, M. Razaviyayn, Z.-Q. Luo, and C. He, "An iteratively weighted MMSE approach to distributed sum-utility maximization for a MIMO interfering broadcast channel," *IEEE Trans. Signal Process.*, vol. 59, no. 9, pp. 4331–4340, Sep. 2011.

[31] K. Shen and W. Yu, "Fractional programming for communication systems—Part II: Uplink scheduling via matching," *IEEE Trans. Signal Process.*, vol. 66, no. 10, pp. 2631–2644, May 2018.

[32] G. Dong, H. Zhang, S. Jin, and D. Yuan, "Energy-efficiency-oriented joint user association and power allocation in distributed massive MIMO systems," *IEEE Trans. Veh. Technol.*, vol. 68, no. 6, pp. 5794–5808, Jun. 2019.

[33] M. Hong, A. Garcia, J. Barrera, and S. G. Wilson, "Joint access point selection and power allocation for uplink wireless networks," *IEEE Trans. Signal Process.*, vol. 61, no. 13, pp. 3334–3347, Jul. 2013.

[34] T. Zhou, Z. Liu, J. Zhao, C. Li, and L. Yang, "Joint user association and power control for load balancing in downlink heterogeneous cellular networks," *IEEE Trans. Veh. Technol.*, vol. 67, no. 3, pp. 2582–2593, Mar. 2018.

[35] M. Guenach, A. A. Gorji, and A. Bourdoux, "A deep neural architecture for real-time access point scheduling in uplink cell-free massive MIMO," *IEEE Trans. Wireless Commun.*, vol. 21, no. 3, pp. 1529–1541, Mar. 2022.

[36] R. Vaze and H. Ganapathy, "Sub-modularity and antenna selection in MIMO systems," *IEEE Commun. Lett.*, vol. 16, no. 9, pp. 1446–1449, Sep. 2012.

[37] *Study on 3D Channel Model for LTE*, Standard (TS) 36.873, Version 12.7.0, 3GPP, Technical Specification, 3rd Generation Partnership Project (3GPP), Dec. 2017.

[38] M. Bashar, K. Cumanan, A. G. Burr, H. Q. Ngo, E. G. Larsson, and P. Xiao, "Energy efficiency of the cell-free massive MIMO uplink with optimal uniform quantization," *IEEE Trans. Green Commun. Netw.*, vol. 3, no. 4, pp. 971–987, Dec. 2019.

[39] H. Q. Ngo, L.-N. Tran, T. Q. Duong, M. Matthaiou, and E. G. Larsson, "On the total energy efficiency of cell-free massive MIMO," *IEEE Trans. Green Commun. Netw.*, vol. 2, no. 1, pp. 25–39, Mar. 2018.

[40] R. Nikbakht, R. Mosayebi, and A. Lozano, "Uplink fractional power control and downlink power allocation for cell-free networks," *IEEE Wireless Commun. Lett.*, vol. 9, no. 6, pp. 774–777, Jun. 2020.

[41] R. Hunger, "An introduction to complex differentials and complex differentiability," Tech. Univ. Munich, Munich, Germany, Tech. Rep. TUM-LNS-TR-07-06, Jul. 2007.

Jiwei Zhao (Member, IEEE) received the M.S. degree in information and communication system from Xidian University, Xi'an, China, in 2018. He is currently working toward the Ph.D. degree with the School of Electronic Science and Engineering, Nanjing University, Nanjing, China. He won the first prize in the 2016 CCF (China Computer Federation) China Big Data and Cloud Computing Intelligence Contest. His research interests include fully-decoupled RAN architecture, coordinated multi-point, and machine learning applications for wireless communication.

Authorized licensed use limited to: University of Waterloo. Downloaded on August 20,2023 at 10:02:36 UTC from IEEE Xplore. Restrictions apply.

Quan Yu (Fellow, IEEE) received the Ph.D. degree in fiber optics from the University of Limoges in 1992. Since 1992, he joined the faculty of the Institute of China Electronic System Engineering Corporation. He is currently a Principal Research Scientist with the Peng Cheng Laboratory. His main areas of research interest are the architecture of wireless networks, optimization of protocols, and cognitive radios. He is an Academician of the Chinese Academy of Engineering (CAE) and the founding Editor-in-Chief of the *Journal of Communications and Information Networks*.

Bo Qian (Member, IEEE) received the B.S. and M.S. degrees in statistics from Sichuan University, Chengdu, China, in 2015 and 2018, and the Ph.D. degree in information and communication engineering from Nanjing University, Nanjing, China, in 2022, respectively. He is currently a Postdoctoral Fellow with Peng Cheng Laboratory, Shenzhen, China. His research interests include resource management in B5G/6G networks, VANET, network economics, blockchain and game theory. He was a recipient of the Best Paper Award from IEEE VTC2020-Fall.

Kai Yu (Student Member, IEEE) received the B.S. degree in detection, guidance, and control technology from the University of Electronic Science and Technology of China, Chengdu, China, in 2019. He is currently pursuing the Ph.D. degree with the School of Electronic Science and Engineering, Nanjing University, China. His research interests include resource allocation, machine learning for wireless communications, and heterogeneous networks.

Yunting Xu (Student Member, IEEE) received the B.S. degree in communication engineering from Nanjing University, Nanjing, China in 2017. He is currently pursuing the Ph.D. degree with the School of Electronic Science and Engineering, Nanjing University, China. He mainly focuses on the wireless network access, dynamic resource management, and personalized wireless service in the field of next generation wireless networks.

Haibo Zhou (Senior Member, IEEE) received the Ph.D. degree in information and communication engineering from Shanghai Jiao Tong University, Shanghai, China, in 2014. From 2014 to 2017, he was a Postdoctoral Fellow with the Broadband Communications Research Group, Department of Electrical and Computer Engineering, University of Waterloo. He is currently a Full Professor with the School of Electronic Science and Engineering, Nanjing University, Nanjing, China. He was a recipient of the 2019 IEEE ComSoc Asia-Pacific Outstanding Young Researcher Award. He served as Track/Symposium Co-Chair for IEEE/CIC ICCC 2019, IEEE VTC-Fall 2020, IEEE VTC-Fall 2021, and IEEE GLOBECOM 2022. He is currently an Associate Editor of the IEEE TRANSACTIONS ON WIRELESS COMMUNICATIONS, IEEE INTERNET OF THINGS JOURNAL, *IEEE Network* Magazine, and IEEE WIRELESS COMMUNICATIONS LETTER. His research interests include resource management and protocol design in B5G/6G networks, vehicular ad hoc networks, and space-air-ground integrated networks.

Xuemin (Sherman) Shen (Fellow, IEEE) received the Ph.D. degree in electrical engineering from Rutgers University, New Brunswick, NJ, USA, in 1990. He is a University Professor with the Department of Electrical and Computer Engineering, University of Waterloo, Canada. His research focuses on network resource management, wireless network security, Internet of Things, 5G and beyond, and vehicular ad hoc and sensor networks.

Dr. Shen is a registered Professional Engineer of Ontario, Canada, an Engineering Institute of Canada Fellow, a Canadian Academy of Engineering Fellow, a Royal Society of Canada Fellow, a Chinese Academy of Engineering Foreign Member, and a Distinguished Lecturer of the IEEE Vehicular Technology Society and Communications Society. Dr. Shen received the Canadian Award for Telecommunications Research from the Canadian Society of Information Theory (CSIT) in 2021, the R.A. Fessenden Award in 2019 from IEEE, Canada, Award of Merit from the Federation of Chinese Canadian Professionals (Ontario) in 2019, James Evans Avant Garde Award in 2018 from the IEEE Vehicular Technology Society, Joseph LoCicero Award in 2015 and Education Award in 2017 from the IEEE Communications Society, and Technical Recognition Award from Wireless Communications Technical Committee (2019) and AHSN Technical Committee (2013). He has also received the Excellent Graduate Supervision Award in 2006 from the University of Waterloo and the Premiers Research Excellence Award (PREA) in 2003 from the Province of Ontario, Canada. He served as the Technical Program Committee Chair/CoChair for IEEE Globecom 16, IEEE Infocom14, IEEE VTC10 Fall, IEEE Globecom07, and the Chair for the IEEE Communications Society Technical Committee onWireless Communications. Dr. Shen is the President of the IEEE Communications Society. He was the Vice President for Technical & Educational Activities, Vice President for Publications, Member-at-Large on the Board of Governors, Chair of the Distinguished Lecturer Selection Committee, Member of IEEE Fellow Selection Committee of the ComSoc. Dr. Shen served as the Editor-in-Chief of the IEEE IoT JOURNAL, *IEEE Network*, and *IET Communications*.

Authorized licensed use limited to: University of Waterloo. Downloaded on August 20,2023 at 10:02:36 UTC from IEEE Xplore. Restrictions apply.